Comparative analysis of beam models for vertical rail vibrations under dynamic forces

Le-Hung Tran, Tuan-Manh Duong, Benjamin Claudet, Khuong Le-Nguyen, Anders Nordborg, Franziska Schmidt

Comparative analysis of beam models for vertical rail vibrations under dynamic forces

Le-Hung Tran[a], Tuan-Manh Duong[b], Benjamin Claudet[c], Khuong Le-Nguyen[d,e], Anders Nordborg[f], Franziska Schmidt[a]

[a] *Université Gustave Eiffel, MAST/EMGCU, 5 Boulevard Descartes, Champs-sur-Marne, 77420, Seine-et-Marne, France*
[b] *Faculty of Civil Engineering, University of Engineering and Technology (UET), VNU-Hanoi, 144 Xuan Thuy, Cau Giay District, Hanoi, Vietnam*
[c] *Laboratoire Navier, UMR 8205, École des Ponts ParisTech, Université Gustave Eiffel, CNRS, 6-8 avenue Blaise Pascal, Champs-sur-Marne, 77420, Seine-et-Marne, France*
[d] *Faculty of Arts & Design, University of Canberra, 11 Kirinari Str, Bruce ACT, 2617, Australia*
[e] *Department of Civil Engineering, University of Transport Technology (UTT), 54 Trieu Khuc, Thanh Xuan District, Hanoi, Vietnam*
[f] *Sound View Instruments AB, Borrby, SE-27636, Sweden*

Abstract

An analytical model of the rails of ballasted railway track subjected to the dynamic loads are developed to study forced vertical vibration. In this work, the two rails are modelled as infinite uniform beams posed on a system of periodical supports with the help of Timoshenko beam theory. Besides, each support is considered as a beam posed on a visco-elastic foundation. A linear relation between the sleeper displacement at the crossing-points with two rails and the two reaction forces is established via the Green's function in the frequency domain. In other words, the mechanical behaviour of the support can be written as a spring with an equivalent stiffness. By replacing this relation into the periodically supported rail models, the forced vertical vibrations of two rails are obtained analytically. This analytical model allows calculate rapidly the rail responses in different load, especially in the non-symmetric configuration. In addition, the comparison of rail responses calculated by two beam models are investigated. This work concerns the study of peaks

*Corresponding author
Email address: le-hung.tran@univ-eiffel.fr (Le-Hung Tran)

resonances of the frequency responses functions which is useful to understand the excitations of rolling noise.

Keywords: Dynamic structure, Vibrations, Railway track, Euler-Bernoulli beam, Kelvin-Voigt foundation, periodically supported beam, Green's function, dynamic loads
PACS: 0000, 1111
2000 MSC: 0000, 1111

---

1. Introduction

Railways are increasingly viewed as a green transport option, sparking significant interest in their expanded role in freight movement, high-speed passenger travel, and congestion relief in urban areas via the implementation of light rail and tramway systems. With advancements in speed and capacity, both intercity and urban rail systems are entering a new phase, poised to mitigate the environmental impact of growing road transport. However, the promotion of rail can face setbacks due to the adverse environmental impacts of track vibration and noise. It should be noted that the vibration characteristics and sound radiation characteristics show a certain correlation with each other. Therefore, within the railway community, there's a rising recognition of the necessity for vibration reduction methods at the source. It's essential to deepen the fundamental understanding of the mechanisms that generate vibration (and noise). Among the sources of railway noise, this paper focuses on the forced vertical vibration of the ballasted railway track subjected to excitation loads representing the irregularities in wheel/rail contacts. [1].

The theoretical models for railway tracks have been developed since the 1970s, initially based on an infinite beam on a continuous foundation [2]. However, these simple models still have limitations due to the absence of a support system. Consequently, models featuring an infinite beam on discrete supports, known as periodically supported beam models, were developed. Hoang et al. calculated the dynamic responses of rails to moving loads using Floquet's theorem and Fourier's transform [3–5], demonstrating a linear relationship between reaction force and rail displacement in the frequency domain. This relationship enabled the development of theoretical models for mono-block sleepers subjected to moving loads [6–9]. The dynamic behaviour of sleepers has been studied through various methods, including numerical approaches by Kaewunruen et al. [10] [11], Grassie [12], and experimental

methods by Park et al. [13] or Janeliukstis [14]. Nordborg's track models [15–19] permit the study of the effect of moving loads on vertical rail vibrations with an analytical approach. However, the validity of these developments is limited by Euler-Bernoulli's beam theory [20]. To address this, Nordborg introduced corrections to the bending stiffness of the models to validate track responses at pinned-pinned frequency. Rail vibrations are also studied in cases of random sleeper spacing by Heckl [21]. Vertical rail vibration has been investigated by numerous researchers, including Grassie [22, 23], Knothe [24], Mead [25–28], Yin et al. [29], Kumawat [30] and Tran et al. [31].

However, the mentioned theoretical models for railway tracks typically focus on a single beam, whereas the actual track consists of two rails fixed by a system of periodic supports. This discrepancy poses a challenge addressed through numerical methods, particularly Finite Element Method (FEM) simulations [32–37]. Recently, Sadegi [38] employed numerical techniques, considering the non-linear effects of the foundation, to model railway tracks. Ruiz et al. [39] investigated ground vibrations induced by railway traffic using a 3D FEM model. Moreover, studies on ground vibration within the MOTIV project context have been conducted [40–46]. Advanced numerical methods have been employed to reduce computation time. Tran et al. [47–49] explored the influence of non-homogeneous and non-linear foundations on railway sleeper responses by developing a semi-analytical model for the complete railway track. Claudet et al. [50] and Yang et al. [51] developed numerical models of the track using the Wave Finite Element Method (WFEM), which is based on wave propagation and attenuation in periodically supported rails. While numerical methods offer significant advantages, such as accuracy, they are limited by computation time.

Therefore, this study focuses on analytically calculating the forced vibrations of the two rails of the track under dynamic loads. Assuming identical supports, each modeled as a beam on a viscoelastic foundation, a relationship between the reaction force applied on the sleeper and the displacement is established using Green's function in the frequency domain. In other words, each support is also treated as a spring with an equivalent stiffness depending on the mechanical parameters of the sleeper, foundation, and rail pad. Additionally, each rail is modeled as an infinite beam with constant section following the Timoshenko beam model. By incorporating these results into the model, the forced vibration of the two rails is analytically obtained using Floquet's theorem (condition of track periodicity) in the frequency domain.

The calculation details are provided in Section 2. Section 3 presents numerical examples comparing the dynamic responses of the rails obtained by two beam theories. Finally, concluding remarks are drawn in Section 4.

2. Theory

Let us consider the representation of the ballasted railway track in 3D as shown in Fig 1. In this figure, the track contains two rails which are placed on a system of periodic supports with an inter-support distance of l. Two dynamic loads, Q_1 and Q_2, are applied to the two rails at positions x_{r_1} and x_{r_2}, respectively. The solution to the problem is calculated by developing two following models: a model of a beam posed on a viscoelastic foundation for the sleeper and a model of a periodically supported beam for the rails.

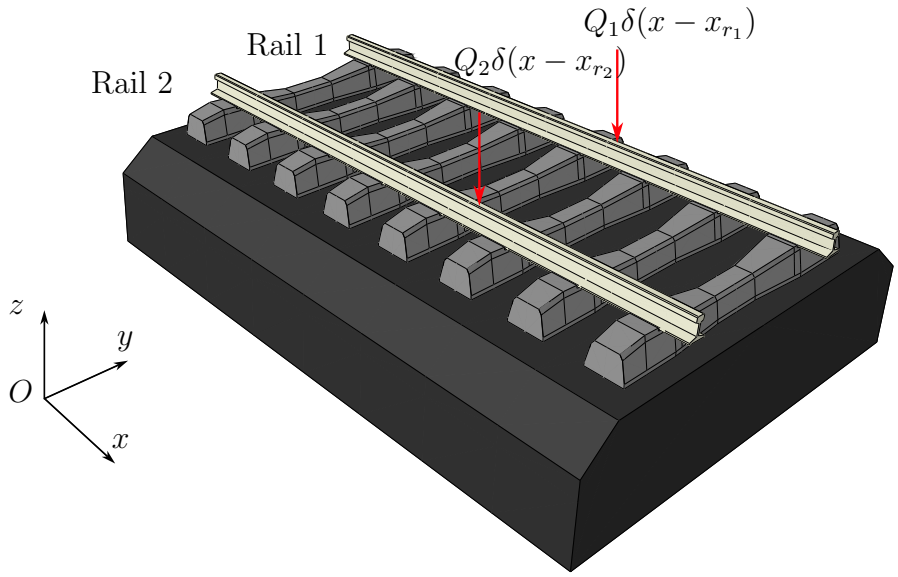

Figure 1: Representation of the ballasted railway track

2.1. Analytical model of railway sleepers

2.1.1. Dynamic equation of an Euler-Bernoulli beam posed on visco-elastic foundation

The Fig. 2 illustrates the analytical representation of the sleeper in the (Oyz) plane. The sleeper is modeled as a uniform Euler-Bernoulli beam with a length of $2L$ ($y \in [-L, L]$). In practical scenarios, the sleeper is embedded

within the ballast layer. For the sake of simplifying the research problem addressed in this paper, we assume the sleeper to be a free-free at each end of the beam, positioned on a visco-elastic foundation characterized by the stiffness k_b and damping coefficient ζ_b.

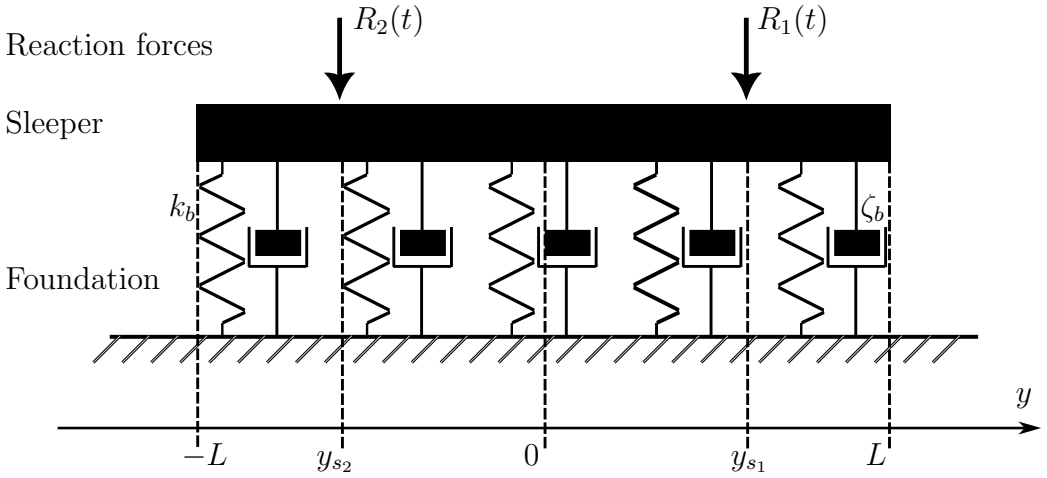

Figure 2: Representation of the dynamical model of the sleepers

Two vertical forces, $R_{1,2}(t)$, are applied to the beam at two positions: y_{s_1} and y_{s_2}, corresponding to the two crossing-points with rails 1 and 2, respectively. The dynamic equation of the beam, expressed in terms of the vertical beam displacement $u_s(y,t)$ and utilizing the Dirac delta distribution, is given by:

$$B_s\frac{\partial^4 u_s}{\partial y^4} + M_s\frac{\partial^2 u_s}{\partial t^2} + k_b u_s + \zeta_b\frac{\partial u_s}{\partial t} = -R_1(t)\delta(y-y_{s_1}) - R_2(t)\delta(y-y_{s_2}) \quad (1)$$

where B_s, M_s are the flexural rigidity and linear mass density of sleeper. By performing the Fourier transform, Eq. (1) is given in the frequency domain where $\hat{u}_s(y,\omega)$ is the vertical displacement of rail in the frequency domain as follows:

$$\mathcal{L}_s\left(\hat{u}_s\right) = -\frac{\hat{R}_1(\omega)}{B_s}\delta(y-y_{s_1}) - \frac{\hat{R}_2(\omega)}{B_s}\delta(y-y_{s_2}) \quad (2)$$

where the mathematical operator $\mathcal{L}_s$ is defined in Eq. (A.3). The vertical external forces applied on the beam at two positions in the frequency domain are: $\hat{R}_{1,2}(\omega)$. Eq. (2) is a 4^{th} order linear differential equation where the

solution can be obtained with the help of Green's function: $\hat{G}_s^{y_{s_{1,2}}}(y,\omega)$. The definition of the two Green's functions are detailed in Appendix A.1. Hence, the sleeper displacement is given by:

$$\hat{u}_s(y,\omega) = -\hat{R}_1(\omega)\hat{G}_s^{y_{s_1}}(y,\omega) - \hat{R}_2(\omega)\hat{G}_s^{y_{s_2}}(y,\omega) \tag{3}$$

Therefore, we can deduce the sleeper displacements at two load positions:

$$\begin{cases} \hat{u}_s(y_{s_1},\omega) = -\hat{R}_1(\omega)\hat{G}_s^{y_{s_1}}(y_{s_1},\omega) - \hat{R}_2(\omega)\hat{G}_s^{y_{s_2}}(y_{s_1},\omega) \\ \hat{u}_s(y_{s_2},\omega) = -\hat{R}_1(\omega)\hat{G}_s^{y_{s_1}}(y_{s_2},\omega) - \hat{R}_2(\omega)\hat{G}_s^{y_{s_2}}(y_{s_2},\omega) \end{cases} \tag{4}$$

It should be noted that in the homogeneous foundation with symmetric configuration of loads: $y_{s_1} = -y_{s_2} = y_s$, so we can deduce the following relation of the two Green's functions:

$$\begin{cases} \hat{G}_s^{y_{s_1}}(y_{s_1},\omega) = \hat{G}_s^{y_{s_2}}(y_{s_2},\omega) = \hat{G}_s^{y_s}(y_s,\omega) \\ \hat{G}_s^{y_{s_1}}(y_{s_2},\omega) = \hat{G}_s^{y_{s_2}}(y_{s_1},\omega) = \hat{G}_s^{y_s}(-y_s,\omega) \end{cases} \tag{5}$$

2.1.2. Rail-pads at the crossing-points

Rail-pads are positioned between the rails and sleepers (at crossing-points) to shield the sleepers from the impact of the rail as the train passes by. This component may exhibit non-linear mechanical behaviours; however, for the purposes of this study, we assume that it can be represented as a massless spring-damper system with specific stiffness k_{rp} and damping coefficients ζ_{rp}. Its dynamic stiffness $\hat{k}_{rp}(\omega)$ is calculated in the frequency domain as follows:

$$\hat{k}_{rp}(\omega) = k_{rp} + \mathrm{i}\omega\zeta_{rp} \tag{6}$$

Now, we focus on one specific railway sleeper, for example at the reference support ($x = 0$), the displacement of sleeper is noted as $\hat{u}_{s_0}(y,\omega)$. Besides, the displacements of rails 1 and 2 in the frequency domain are $\hat{u}_{r_1}(0,\omega)$ and $\hat{u}_{r_2}(0,\omega)$, respectively. It should be noted that the rail-pads are considered as a linear spring in the frequency. Thus, the reaction force and the variation of length are linked via the dynamic stiffness. Hence, the reaction force applied on this sleeper are calculated:

$$\begin{cases} \hat{R}_1(\omega) = \hat{k}_{rp}\left[\hat{u}_{r_1}(0,\omega) - \hat{u}_{s_0}(y_{s_1},\omega)\right] \\ \hat{R}_2(\omega) = \hat{k}_{rp}\left[\hat{u}_{r_2}(0,\omega) - \hat{u}_{s_0}(y_{s_2},\omega)\right] \end{cases} \tag{7}$$

By replacing Eqs. (7) and (5) into Eq. (4), we establish a relation between the displacement of sleeper and rails at the crossing-points (see (Appendix A.2)):

$$\begin{cases} \hat{u}_{s_0}(y_s,\omega) & = \mathcal{G}_1(\omega)\hat{u}_{r_1}(0,\omega) + \mathcal{G}_2(\omega)\hat{u}_{r_2}(0,\omega) \\ \hat{u}_{s_0}(-y_s,\omega) & = \mathcal{G}_2(\omega)\hat{u}_{r_1}(0,\omega) + \mathcal{G}_1(\omega)\hat{u}_{r_2}(0,\omega) \end{cases} \tag{8}$$

We suppose that the supports are identical, therefore, Eq. (8) is valid not only for the reference $x = 0$ but also for any sleeper n at coordinate $x = nl$, where l is the distance between two supports and $n \in \mathbb{Z}$. In addition, with the help of the Dirac delta distribution, we have:

$$\begin{cases} \hat{u}_{s_n}(y_s,\omega) & = \left[\mathcal{G}_1(\omega)\hat{u}_{r_1}(x,\omega) + \mathcal{G}_2(\omega)\hat{u}_{r_2}(x,\omega)\right]\delta(x-nl) \\ \hat{u}_{s_n}(-y_s,\omega) & = \left[\mathcal{G}_2(\omega)\hat{u}_{r_1}(x,\omega) + \mathcal{G}_1(\omega)\hat{u}_{r_2}(x,\omega)\right]\delta(x-nl) \end{cases} \tag{9}$$

Finally, Eq. (9) leads to the following relation:

$$\begin{cases} \hat{u}_{s_n}(y_s,\omega) + \hat{u}_{s_n}(-y_s,\omega) = \left[\mathcal{G}_1(\omega) + \mathcal{G}_2(\omega)\right]\left[\hat{u}_{r_1}(x,\omega) + \hat{u}_{r_2}(x,\omega)\right]\delta(x-nl) \\ \qquad\qquad = \mathcal{G}_+(\omega)\hat{u}_{r_+}(x,\omega)\delta(x-nl) \\ \hat{u}_{s_n}(y_s,\omega) - \hat{u}_{s_n}(-y_s,\omega) = \left[\mathcal{G}_1(\omega) - \mathcal{G}_2(\omega)\right]\left[\hat{u}_{r_1}(x,\omega) - \hat{u}_{r_2}(x,\omega)\right]\delta(x-nl) \\ \qquad\qquad = \mathcal{G}_-(\omega)\hat{u}_{r_-}(x,\omega)\delta(x-nl) \end{cases} \tag{10}$$

2.2. Analytical model for the railway track

2.2.1. Model of periodically supported beam subjected to a point-force

Each rail on the track is conceptualized as an infinitely long, uniform beam situated in the (Oxz) plane. It is supported by a system of periodic and identical supports, as depicted in Fig. 3.

The mechanical characteristics of the rail align with the principles of the Timoshenko beam theory. Under the assumption that both rails possess identical mechanical properties, the dynamic equations governing the response of the two rails to the normal forces $F_{r_{1,2}}(x,t)$ (applied to rail 1 and 2, respectively) are articulated in the ensuing system of equations:

$$\begin{cases} M_r\dfrac{\partial^2 u_{r_1}}{\partial t^2} = K_r\left(\dfrac{\partial^2 u_{r_1}}{\partial x^2} - \dfrac{\partial \phi_{r_1}}{\partial x}\right) + F_{r_1} \\ J_r\dfrac{\partial^2 \phi_{r_1}}{\partial t^2} = B_r\dfrac{\partial^2 \phi_{r_1}}{\partial x^2} + K_r\left(\dfrac{\partial u_{r_1}}{\partial x} - \phi_{r_1}\right) \\ M_r\dfrac{\partial^2 u_{r_2}}{\partial t^2} = K_r\left(\dfrac{\partial^2 u_{r_2}}{\partial x^2} - \dfrac{\partial \phi_{r_2}}{\partial x}\right) + F_{r_2} \\ J_r\dfrac{\partial^2 \phi_{r_2}}{\partial t^2} = B_r\dfrac{\partial^2 \phi_{r_2}}{\partial x^2} + K_r\left(\dfrac{\partial u_{r_2}}{\partial x} - \phi_{r_2}\right) \end{cases} \tag{11}$$

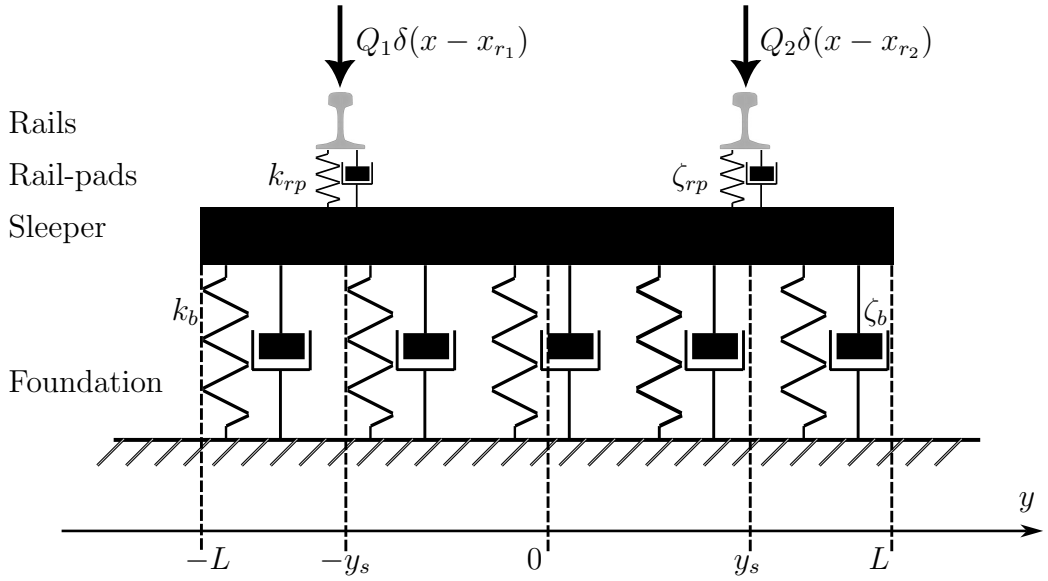

Figure 3: Representation of the dynamic model for the ballasted railway track

where $u_{r_{1,2}}(x,t)$, $\phi_{r_{1,2}}(x,t)$ are the vertical displacement and rotational section of the rails 1 and 2 in the time domain, respectively. The coefficients B_r, M_r, J_r and K_r are the flexural rigidity, linear mass density, rotational inertia and shear rigidity of rail, respectively.

By performing the Fourier's transform, Eq. (11) is given in the frequency domain:

$$\begin{cases} \mathcal{L}_r(\hat{u}_{r_1}) = \dfrac{1}{B_r}\left[1 - \dfrac{B_r}{K_r}\left(\dfrac{\partial^2}{\partial x^2} + \dfrac{J_r}{B_r}\omega^2\right)\right]\hat{F}_{r_1} \\ \mathcal{L}_r(\hat{\phi}_{r_1}) = \dfrac{1}{B_r}\dfrac{\partial}{\partial x}\hat{F}_{r_1} \\ \mathcal{L}_r(\hat{u}_{r_2}) = \dfrac{1}{B_r}\left[1 - \dfrac{B_r}{K_r}\left(\dfrac{\partial^2}{\partial x^2} + \dfrac{J_r}{B_r}\omega^2\right)\right]\hat{F}_{r_2} \\ \mathcal{L}_r(\hat{\phi}_{r_2}) = \dfrac{1}{B_r}\dfrac{\partial}{\partial x}\hat{F}_{r_2} \end{cases} \tag{12}$$

where the mathematical operator $\mathcal{L}_r$ is defined in Eq. (B.4). The functions $\hat{u}_{r_{1,2}}(x,\omega)$, $\hat{\phi}_{r_{1,2}}(x,\omega)$, and $\hat{F}_{r_{1,2}}(x,\omega)$ represent the vertical displacement, rotational section, and normal forces applied on rails 1 and 2 in the frequency domain, respectively. Eq. (12) describes the dynamic responses of the two rails in the frequency domain. The total vertical normal forces applied on the rails $\hat{F}_{r_{1,2}}(x,\omega)$ consist of reaction forces from the support system $\hat{F}_{s_{1,2}}(x,\omega)$

and the loads from the train $\hat{F}_{t_{1,2}}(x,\omega)$ which the relations are expressed as follows (see Eq. (B.5)):

$$\begin{cases} \hat{F}_{r_1}(x,\omega) = \hat{F}_{t_1}(x,\omega) - \hat{F}_{s_1}(x,\omega) \\ \hat{F}_{r_2}(x,\omega) = \hat{F}_{t_2}(x,\omega) - \hat{F}_{s_2}(x,\omega) \end{cases} \tag{13}$$

As previously stated, the supports are assumed to be identical, and the total reaction forces at coordinates $x = nl$ are calculated as follows:

$$\begin{cases} \hat{F}_{s_1} = \displaystyle\sum_{n=-\infty}^{\infty} \hat{k}_b \left[\hat{u}_{r_1}(nl,\omega) - \hat{u}_{s_n}(y_{s_1},\omega)\right] = \sum_{n=-\infty}^{\infty} \hat{k}_b \left[\hat{u}_{r_1}(0,\omega) - \hat{u}_{s_n}(y_s,\omega)\right] \delta(x-nl) \\ \hat{F}_{s_2} = \displaystyle\sum_{n=-\infty}^{\infty} \hat{k}_b \left[\hat{u}_{r_2}(nl,\omega) - \hat{u}_{s_n}(y_{s_2},\omega)\right] = \sum_{n=-\infty}^{\infty} \hat{k}_b \left[\hat{u}_{r_2}(0,\omega) - \hat{u}_{s_n}(-y_s,\omega)\right] \delta(x-nl) \end{cases} \tag{14}$$

It should be noted that the reaction forces depend on the vertical displacements of rails and supports, as shown in Eq. (14).

2.2.2. Coupling of two models and solution of the problem

Eq. (12) describes the responses dynamics of the two rails and it can be written in the following system:

$$\begin{cases} \mathcal{L}_r(\hat{u}_{r_+}) = \mathcal{L}_r(\hat{u}_{r_1} + \hat{u}_{r_2}) = \dfrac{1}{B_r}\left[1 - \dfrac{B_r}{K_r}\left(\dfrac{\partial^2}{\partial x^2} + \dfrac{J_r}{B_r}\omega^2\right)\right]\left(\hat{F}_{r_1} + \hat{F}_{r_2}\right) \\ \mathcal{L}_r(\hat{\phi}_{r_+}) = \mathcal{L}_r(\hat{\phi}_{r_1} + \hat{\phi}_{r_2}) = \dfrac{1}{B_r}\dfrac{\partial}{\partial x}\left(\hat{F}_{r_1} + \hat{F}_{r_2}\right) \\ \mathcal{L}_r(\hat{u}_{r_-}) = \mathcal{L}_r(\hat{u}_{r_1} - \hat{u}_{r_2}) = \dfrac{1}{B_r}\left[1 - \dfrac{B_r}{K_r}\left(\dfrac{\partial^2}{\partial x^2} + \dfrac{J_r}{B_r}\omega^2\right)\right]\left(\hat{F}_{r_1} - \hat{F}_{r_2}\right) \\ \mathcal{L}_r(\hat{\phi}_{r_-}) = \mathcal{L}_r(\hat{\phi}_{r_1} - \hat{\phi}_{r_2}) = \dfrac{1}{B_r}\dfrac{\partial}{\partial x}\left(\hat{F}_{r_1} - \hat{F}_{r_2}\right) \end{cases}$$

(15a)

(15b)

In other hand, by substituting Eqs. (10) and (14) into Eq. (13), the following results are deduced:

$$\begin{cases} \hat{F}_{r_+} = \hat{F}_{r_1} + \hat{F}_{r_2} = \left(\hat{F}_{t_1} + \hat{F}_{t_2}\right) - \left(\hat{F}_{s_1} + \hat{F}_{s_2}\right) = \hat{F}_{t_+} - \mathcal{K}_+ \sum_{n=-\infty}^{\infty} \hat{u}_{r_+}\delta(x-nl) \\ \hat{F}_{r_-} = \hat{F}_{r_1} - \hat{F}_{r_2} = \left(\hat{F}_{t_1} - \hat{F}_{t_2}\right) - \left(\hat{F}_{s_1} - \hat{F}_{s_2}\right) = \hat{F}_{t_-} - \mathcal{K}_- \sum_{n=-\infty}^{\infty} \hat{u}_{r_-}\delta(x-nl) \end{cases} \tag{16}$$

where:

$$\begin{cases} \mathcal{K}_+(\omega) = \hat{k}_b(\omega)\left(1 - \mathcal{G}_+(\omega)\right) \\ \mathcal{K}_-(\omega) = \hat{k}_b(\omega)\left(1 - \mathcal{G}_-(\omega)\right) \end{cases}$$

Finally, by replacing the previous result into Eq.(12), this system of equations is expressed as:

$$\begin{cases} \mathcal{L}_r(\hat{u}_{r_+}) - \dfrac{\mathcal{K}_+}{B_r}\left[1 - \dfrac{B_r}{K_r}\left(\dfrac{\partial^2}{\partial x^2} + \dfrac{J_r}{B_r}\omega^2\right)\right] \sum_{n=-\infty}^{\infty} \hat{u}_{r_+}\delta(x-nl) \\ = \dfrac{1}{B_r}\left[1 - \dfrac{B_r}{K_r}\left(\dfrac{\partial^2}{\partial x^2} + \dfrac{J_r}{B_r}\omega^2\right)\right] \hat{F}_{t_+} \qquad (17a) \\ \mathcal{L}_r(\hat{\phi}_{r_+}) - \dfrac{\mathcal{K}_+}{B_r}\dfrac{\partial}{\partial x} \sum_{n=-\infty}^{\infty} \hat{u}_{r_+}\delta(x-nl) = \dfrac{1}{B_r}\dfrac{\partial}{\partial x}\hat{F}_{t_+} \\ \mathcal{L}_r(\hat{u}_{r_-}) - \dfrac{\mathcal{K}_-}{B_r}\left[1 - \dfrac{B_r}{K_r}\left(\dfrac{\partial^2}{\partial x^2} + \dfrac{J_r}{B_r}\omega^2\right)\right] \sum_{n=-\infty}^{\infty} \hat{u}_{r_-}\delta(x-nl) \\ = \dfrac{1}{B_r}\left[1 - \dfrac{B_r}{K_r}\left(\dfrac{\partial^2}{\partial x^2} + \dfrac{J_r}{B_r}\omega^2\right)\right] \hat{F}_{t_-} \qquad (17b) \\ \mathcal{L}_r(\hat{\phi}_{r_-}) - \dfrac{\mathcal{K}_-}{B_r}\dfrac{\partial}{\partial x} \sum_{n=-\infty}^{\infty} \hat{u}_{r_-}\delta(x-nl) = \dfrac{1}{B_r}\dfrac{\partial}{\partial x}\hat{F}_{t_-} \end{cases}$$

The previously established system of equations shares the same form as that developed in Eq. (B.7). It is important to note that train loads consist of two components: static and dynamic loads. However, this paper specifically concentrates on the responses of rails under dynamic loads $\hat{F}_{t_{1,2}}(x,\omega)$, which are categorized as:

$$\begin{cases} \hat{F}_{t_1}(x,\omega) = Q_1\delta(x - x_{r_1}) \\ \hat{F}_{t_2}(x,\omega) = Q_2\delta(x - x_{r_2}) \end{cases} \tag{18}$$

where Q_1 and Q_2 are two constants representing two point forces simultaneously exciting the rails. By replacing Eq. (18) into Eq. (17), we observe that the dynamic responses of the problem are clearly defined, as illustrated in Appendix B.2.2. Hence, the forced vertical vibrations of the two rails are deduced easily from the expressions for $\hat{u}_{r_+}(x,\omega)$ and $\hat{u}_{r_-}(x,\omega)$. By replacing $x = nl$, the vertical displacement of railway sleepers at the crossing-points are obtained with the help of Eq. (9) which permits us to calculate the reaction forces via Eq. (14). The track responses are analytically acquired in the frequency domain, and the corresponding time domain responses can be derived using inverse Fourier transforms.

3. Numerical examples

3.1. Comparison of the model

Firstly, comparing the rail responses obtained from the developed model with those calculated in existing research allows us to confirm the validity of the results. The track parameters are chosen as shown in Table 1. As mentioned earlier, Hamet [20] developed a model of periodically supported rail using Timoshenko theory. However, his development is applicable only to one rail posed on a concrete mono-block. Therefore, the responses of the presented model are calculated in a symmetric configuration, where two unit dynamic loads are applied to the two rails at the same position $x_{r_1} = x_{r_2} = x_0 = l/2$. Additionally, it should be noted that Hamet [20] calculated the dynamic stiffness of the foundation $\hat{k}_b$ and of the railpad $\hat{k}_{rp}$ as follows:

$$\begin{cases} \hat{k}_b = k_b + \mathrm{i}\eta_b \\ \hat{k}_{rp} = k_{rp} + \mathrm{i}\eta_{rp} \end{cases}$$

where η_b and η_{rp} are loss factors of foundation and rail pad, respectively.

Fig. 4 presents a comparison of the evolution of Green's function in the frequency domain at two positions: at the reference support $x = 0$ and at the middle of the period $x = l/2$. In this figure, the two continuous lines correspond respectively to Hamet's model (blue line) and our model (red line). The two dashed-lines show the resonant frequency (green) and pinned-pinned frequency (black) of the track by using Timoshenko beam theory f_{pp}^{TM}.

The resonant frequency (green dashed-line) is obtained: 233.92 Hz with the chosen parameters. This phenomenon can be observed for an infinite

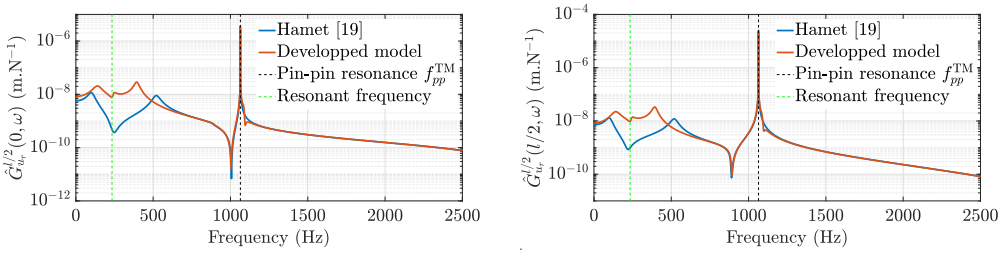

(a) At $x = 0$ (b) At $x = l/2$

Figure 4: Comparison of the evolution of the Green's function in the frequency domain at different positions

beam posed on Winkler foundation and is well explained by Kurze [52]. The frequency where the rail resonance occurs is called the pinned-pinned frequency. In this vibrating mode, the primary motion occurs within the rail itself, with the two supports being regarded as rigid. The first pinned-pinned frequency f_{pp} aligns with the wavelength of the rail bending waves, which is twice the distance between sleepers. The analytical solution of f_{pp} for two beam theories is given as follows:

- For Euler-Bernoulli's beam theory:

$$f_{pp}^{\mathrm{EB}} = \frac{\pi}{2l^2}\sqrt{\frac{B_r}{M_r}} \tag{19}$$

- For Timoshenko beam theory:

$$\begin{aligned} f_{pp}^{\mathrm{TM}} &= \sqrt{\frac{N_r}{8l^2M_r}\left[1+\frac{K_r}{N_r}+\frac{l^2K_r}{\pi^2B_r}-\sqrt{\left(1+\frac{K_r}{N_r}+\frac{l^2K_r}{\pi^2B_r}\right)^2-4\frac{K_r}{N_r}}\right]} \\ &= f_{pp}^{\mathrm{EB}}\sqrt{\frac{l^2N_r}{2\pi^2B_r}\left[1+\frac{K_r}{N_r}+\frac{l^2K_r}{\pi^2B_r}-\sqrt{\left(1+\frac{K_r}{N_r}+\frac{l^2K_r}{\pi^2B_r}\right)^2-4\frac{K_r}{N_r}}\right]} \end{aligned} \tag{20}$$

  where $N_r = E_rS_r$ represents the axial rigidity of the rail.

For the chosen parameters as shown in 3$^{\mathrm{rd}}$ column of Tab. 1, we have: $f_{pp}^{\mathrm{TM}} = 1063.98$ Hz and $f_{pp}^{\mathrm{EB}} = 1386.27$ Hz.

Parameters	Notation	Value		Unit
		Hamet [20]	Present study	
Flexural rigidity of the rail	B_r	6.4	6.3	MNm^2
Linear mass density of the rail	M_r	60	59.98	kgm^{-1}
Rotational inertia of the rail	J_r	0.256	0.234	kgm
Shear rigidity of the rail	K_r	231	269.15	MN
Axial rigidity of the rail	N_r	1500	1614.95	MN
Flexural rigidity of the support	B_s	–	8.13	MNm^2
Linear mass density of the support	M_s	–	145.92	kgm^{-1}
Mass of support	m_s	162	–	kg
Length of the support	$2L$	–	2.41	m
Inter-support distance	l	0.6	0.6	m
Track gauge	–	–	1.435	m
Stiffness of the rail pad	k_{rp}	300	192	MNm^{-1}
Damping coefficient of the rail pad	ζ_{rp}	–	1.97	MNsm^{-1}
Loss factor of the rail pad	η_{rp}	30	–	MNm^{-1}
Stiffness of the foundation	k_b	75	440	MNm^{-1}
Damping coefficient of the foundation	ζ_b	55	58.8	kNsm^{-1}
Loss factor of the foundation	η_b	30	–	MNm^{-1}

Table 1: Track parameters

Fig. 4 illustrates the similarity of results calculated by the two models at high-band frequencies (from 600 Hz). However, it should be noted that the responses differ at low frequencies (from 0 Hz to 500 Hz). This discrepancy can be attributed to the difference in support types. Modeling the support as a beam can induce free vibrations (beam resonances), a phenomenon that does not occur in the case of a mass. Moreover, the sleepers and rail vibrating in phase and out of phase are not obviously the same with two configurations. Nonetheless, both models yield the same resonant frequency and pin-pin resonance f_{pp}^{TM}.

Fig. 5 shows the comparison of Green's function calculated two beam models as function of position x at two frequencies: at $f = 750$ Hz - Fig. 5a and at at pinned-pinned frequency f_{pp}^{TM} which is calculated analytically as earlier, $f = 1064$ Hz - Fig. 5b. The blue and red lines are the rail deflection calculated by Hamet and presented model, respectively. The comparison visually demonstrates similar results, with a small difference observed at the

load position, which can be explained by the difference in support type. Overall, the comparison confirms the validity of the presented model. Additionally, given that railway track sleepers are typically in the form of a concrete beam, the difference between the two models at low-band frequencies could yield significant insights and further enrich this research work.

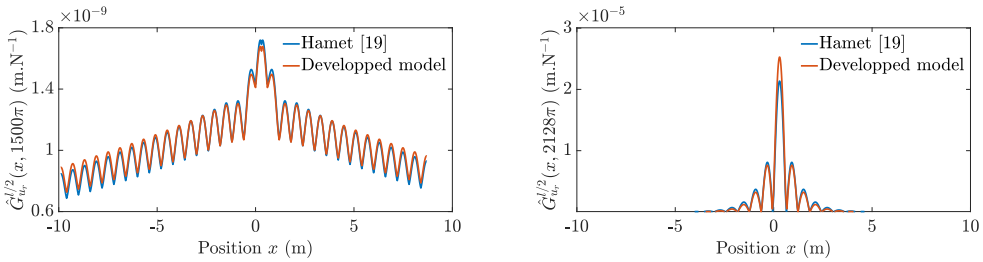

(a) $f = 750$ Hz (b) $f = 1064$ Hz

Figure 5: Comparison of the evolution of the Green's function as function of x at different frequencies

3.2. Influence of beam model choice on the track responses

In the previous Section, the dynamic loads applied on the two rails are considered as symmetric (at the same position $x = l/2$). Therefore, the responses of two rails are obtained obviously symmetric. However, the loads can be applied at two different positions (here, it should be noted that this research paper is limited in the case of two loads applied at the same moment). Hence, we present from now the track responses obtained with dis-symmetric configuration of loads positions: $Q_1 = 1$ at $x_{r_1} = 0$ and $Q_2 = 1$ at $x_{r_2} = l/2$. Moreover, the influence of beam model choice is drawn with the help of Tab. B.2. The notations $(\square)^{\mathrm{EB}}$ and $(\square)^{\mathrm{TM}}$ stand for the Euler-Bernoulli and Timoshenko beam theory, respectively. The subscripts $(\square)_{u_{r_+}}$ and $(\square)_{u_{r_-}}$ denote the results obtained by Eqs. (17a) and (17b), respectively. The parameters chosen are shown in Tab. 1. It should be noted that the pinned-pinned frequencies are slightly changed: $f_{pp}^{\mathrm{EB}} = 1386.27$ Hz and $f_{pp}^{\mathrm{TM}} = 1057.89$ Hz. The two values are presented in Fig. 6 by black continuous and dashed-line.

3.2.1. Track propagation constants

The four propagation coefficients $\gamma_{p,d_\pm}(\omega)$ of the supported rail are illustrated as a function of the frequency as shown in Fig. 6. The continuous-line

and dashed-line are the results of Euler-Bernoulli and Timoshenko beam, respectively. The attenuation of the propagation coefficient is calculated via the Track Decay Rate (TDR), where the formula is given by [53]:

$$\mathrm{TDR}\left(\gamma_{p,d_\pm}(\omega)\right) = -\frac{20}{l}\log_{10}\left(\mathrm{e}^{-\Re\left(\gamma_{p,d_\pm}(\omega)\right)}\right) = -\frac{20}{\ln(10)}\frac{\Re\left(\gamma_{p,d_\pm}(\omega)\right)}{l}$$

where $\Re\left(\gamma_{p,d_\pm}(\omega)\right)$ is the real part of the propagation constants and the inter-support distance l. By convention, the real parts are positive corresponding to the propagating wave direction to the left side.

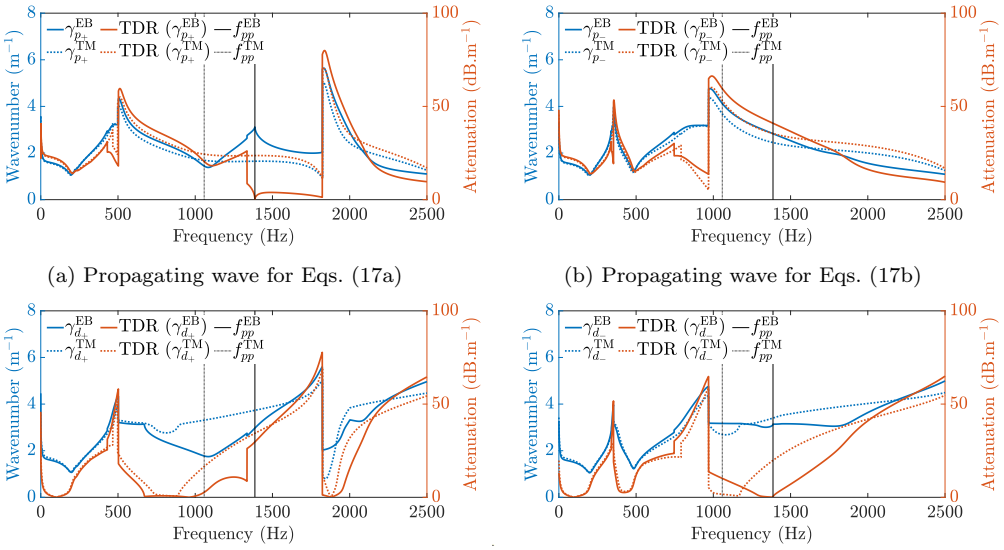

(a) Propagating wave for Eqs. (17a)

(b) Propagating wave for Eqs. (17b)

(c) Near-field wave for Eqs. (17a)

(d) Near-field wave for Eqs. (17b)

Figure 6: Comparison of propagation constants via Eqs. (17) with two beam models

The two propagating waves $\gamma_{p_\pm}(\omega)$ is characterized by a weak attenuation (see Figs. 6a and 6b) meanwhile the near-field waves have a strong attenuation (see Figs. 6c and 6d). The propagation constants calculated by two beam models have almost the same trajectory. The difference appears around the pinned-pinned frequency because of beam theory. These coefficients depend heavily on the stiffness of the support and the track parameters as shown in Appendix B.

3.2.2. Track receptance

The evolution in the frequency domain of the receptance calculated by two beam theories is shown in Fig. 7. In this figure, the track responses cal-

culated by Euler-Bernoulli and Timoshenko beam are presented by the blue and red continuous-lines, respectively. The dashed-lines denote the pinned-pinned frequencies. The first resonant frequency is the same for the two beam model corresponding to the 1$^{\text{st}}$ mode shape of free vibration of the sleeper which is around 195 Hz. In the interval $f \in [0, 700]$ Hz, the trajectory of the two models is quite similar. The difference occurs around the pin-pin resonance which depends strongly on the beam theory. From 1750 Hz, the evolutions of Green's functions obtained by the wo beam theories are quite similar. Particularly, the Timoshenko model exhibits significant resonance at the pinned-pinned frequency f_{pp} regardless of the beam's position (see Figs. 7c, 7d), whereas the Euler-Bernoulli model shows only distinct resonance at the midpoint, $x = l/2$, of the beam (see Figs. 7a, 7b).

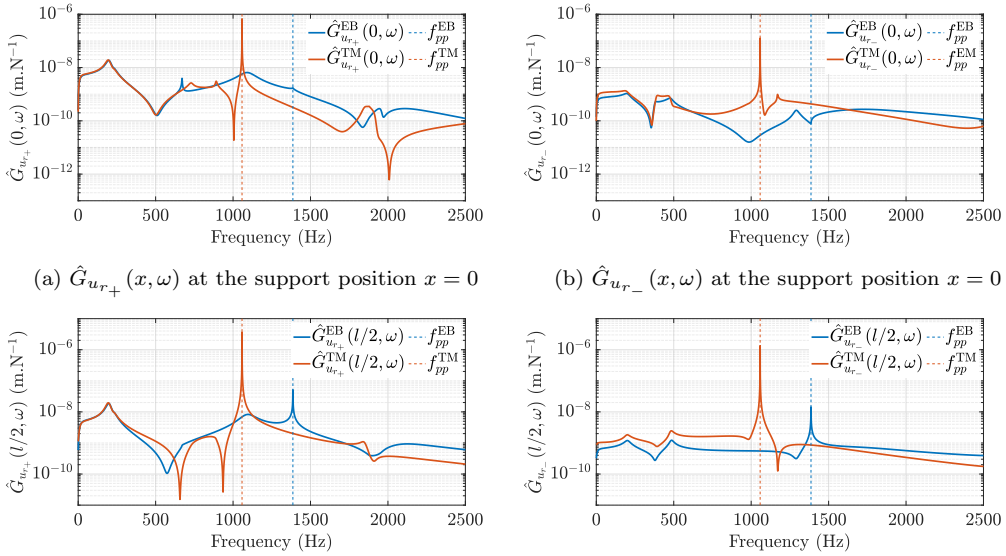

(a) $\hat{G}_{u_{r_+}}(x,\omega)$ at the support position $x = 0$

(b) $\hat{G}_{u_{r_-}}(x,\omega)$ at the support position $x = 0$

(c) $\hat{G}_{u_{r_+}}(x,\omega)$ at the middle of period $x = l/2$

(d) $\hat{G}_{u_{r_-}}(x,\omega)$ at middle of period $x = l/2$

Figure 7: Comparison of Green's function of the ballasted railway track calculated via Eqs. (17) in the function of frequency with two beam models at different positions

The evolutions of the receptance as a function of the position x are illustrated in low frequency, $f = 175$ Hz (Figs. 8a, 8b) and in high frequency, $f = 1750$ Hz (Figs. 8c, 8d). The responses calculated by Timoshenko beam theory attenuate more rapidly than the ones obtained with Euler-Bernoulli beam theory. This phenomenon can be observed clearly at high frequency range. But, around the position $x = 0$ (load position), the $\hat{G}^{\text{TM}}_{u_{r_\pm}}(x,\omega)$ has

the higher values than $\hat{G}^{\mathrm{EB}}_{u_{r_\pm}}(x,\omega)$. For more details, the illustrations in 3D as shown in Appendix C.1 provide the global vision of the evolution of the track Green's function.

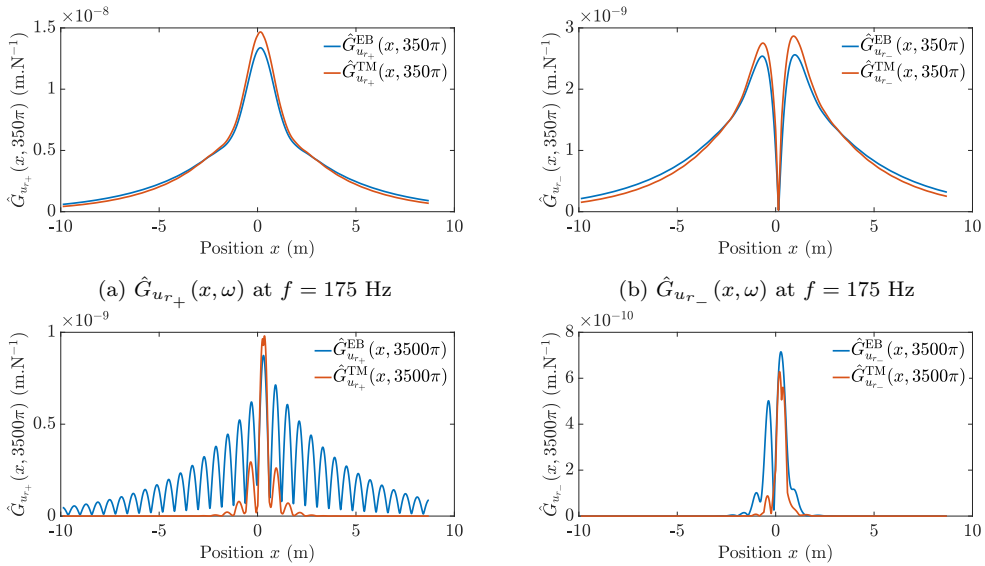

(a) $\hat{G}_{u_{r_+}}(x,\omega)$ at $f = 175$ Hz

(b) $\hat{G}_{u_{r_-}}(x,\omega)$ at $f = 175$ Hz

(c) $\hat{G}_{u_{r_+}}(x,\omega)$ at $f = 1750$ Hz

(d) $\hat{G}_{u_{r_-}}(x,\omega)$ at $f = 1750$ Hz

Figure 8: Comparison of Green's function of the ballasted railway track calculated via Eqs. (17) in the function of x with two beam models at different frequencies

3.2.3. Forced vertical vibrations of the rails

In this Section, the same parameters as earlier are used to calculate the forced vibration of rails at two positions: $x = 0$ (Figs. 9a, 9b) and $x = l/2$ (Figs. 9c, 9d). In these figures, the blue and red lines correspond to the frequency response functions (FRFs) of the rails calculated by the Euler-Bernoulli and Timoshenko beam theory, respectively. The pinned-pinned frequency, which is the same as earlier $f^{\mathrm{EB}}_{pp} = 1386.27$ Hz and $f^{\mathrm{TM}}_{pp} = 1057.89$ Hz, is exhibited by the dashed-line with the same convention of colours.

The most significant peak of FRFs of two rails appear at the pin-pin resonance: f^{EB}_{pp} and f^{TM}_{pp}. It should be noticed that this value dominates the other peaks on the FRFs. This phenomenon demonstrates that the rails vibrate strongly at this frequency. Especially with the ones calculated by Timoshenko, this resonance occurs at all positions of the rails. For the FRFs calculated by Euler-Bernoulli theory, we have a minor resonance at

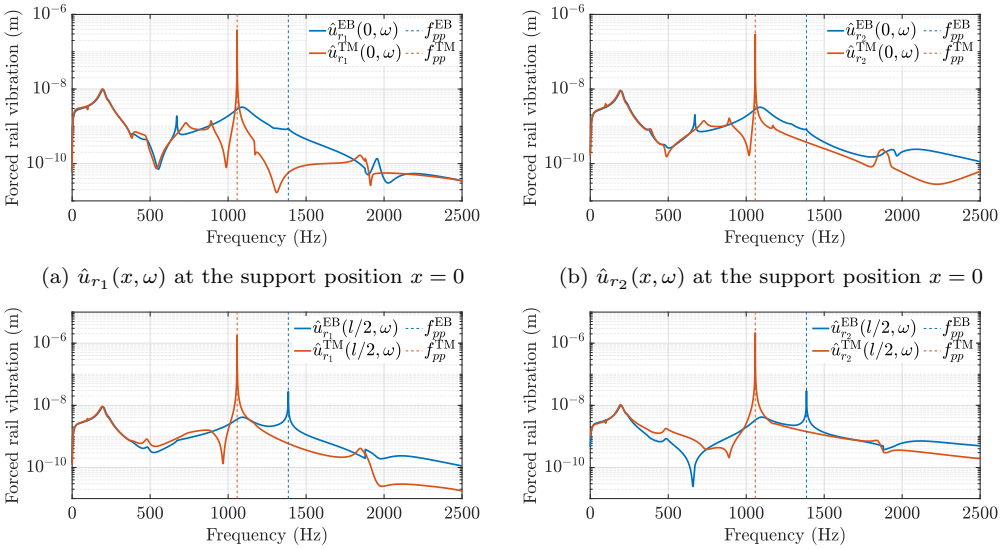

(a) $\hat{u}_{r_1}(x,\omega)$ at the support position $x = 0$

(b) $\hat{u}_{r_2}(x,\omega)$ at the support position $x = 0$

(c) $\hat{u}_{r_1}(x,\omega)$ at the middle of period $x = l/2$

(d) $\hat{u}_{r_2}(x,\omega)$ at the middle of period $x = l/2$

Figure 9: Forced vibrations of two rails under the dynamic loads in the function of frequency domain with two beam models at different positions

the pinned-pinned frequency at the support (see Figs. 9a, 9b). The resonance at the pinned-pinned frequency occurs at the middle of the period $x = l/2$ (see Figs. 9c, 9d).

In the low-frequency range ($f < 750$ Hz), both beam theories exhibit similar responses, characterized by significant peaks: the rail and sleeper oscillate in phase (around 100 Hz), with additional resonances of the sleeper and foundation occurring at around 200 Hz and 480 Hz, respectively. Notably, at $x = 0$, the frequency at which the rail and sleeper oscillate out of phase differs between the two beam theories: approximately 725 Hz for the Timoshenko model and 670 Hz for the Euler-Bernoulli model. Beyond $f = 750$ Hz, significant differences in the Frequency Response Functions (FRFs) between the two beam theories emerge due to the pin-pin resonance. It's important to highlight that the resonance peak of the FRFs of the rails at the pinned-pinned frequency, calculated by the Timoshenko beam model, is notably higher than that of the Euler-Bernoulli beam theory. Moving to the high-frequency range ($f > 1750$ Hz), both theories yield similar responses in the frequency domain. The FRFs exhibit minimal significant peaks due to strong attenuation, as discussed in the track receptance/Green's function

section.

The evolution of the forced vertical rails vibration in the function of x are shown with different frequencies: $f = 200$ Hz (see Figs. 10a, 10b) and $f = 1250$ Hz (see Figs. 10c, 10d). At low frequency, the propagation of the rail vibrations is the same with the two beam theories, as discussed earlier (for example: $f = 200$ Hz). At $f = 1250$ Hz, just after the pinned-pinned frequency, the Timoshenko beam theory demonstrates visually a strong attenuation, even at the load positions. Moreover, following the track direction, the Euler-Bernoulli theory shows slow decay. This phenomenon is also discussed in the track receptance Section. For more details, Appendix C.2 illustrates the evolutions of the forced vertical vibration of two rails in two variables: frequency and position. The resonance peak of the FRFs of the rails at the pinned-pinned frequency calculated by the Timoshenko beam model is much higher than for the Euler-Bernoulli beam theory. The differences of the rail responses obtained by two beam theories are also shown clearly in Appendix C.2.

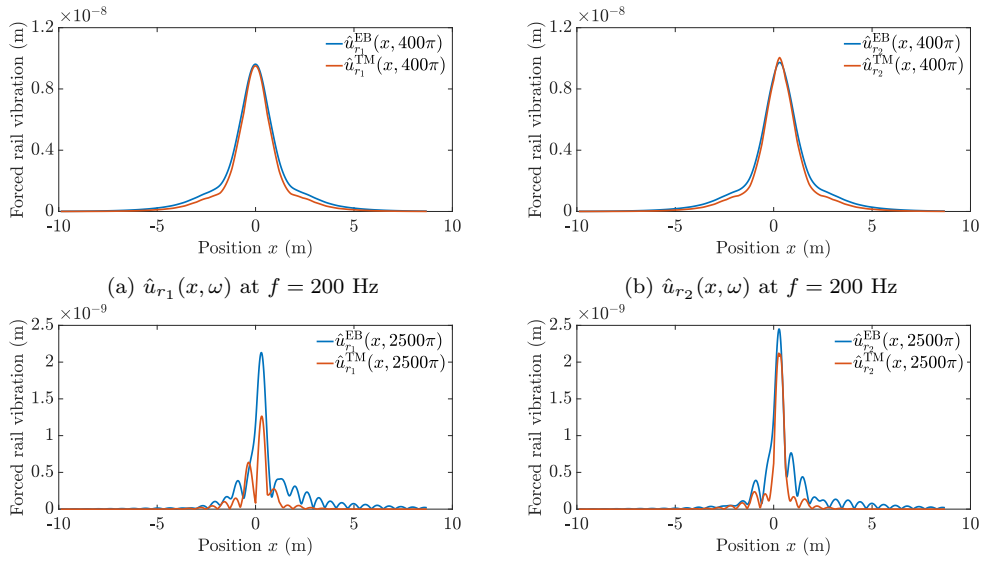

(a) $\hat{u}_{r_1}(x, \omega)$ at $f = 200$ Hz

(b) $\hat{u}_{r_2}(x, \omega)$ at $f = 200$ Hz

(c) $\hat{u}_{r_1}(x, \omega)$ at $f = 1250$ Hz

(d) $\hat{u}_{r_2}(x, \omega)$ at $f = 1250$ Hz

Figure 10: Forced vibrations of two rails under the dynamic loads in the function of x with two beam models at different frequencies

4. Conclusion

This research presents an analytical model for analyzing the dynamic behavior of ballasted railway tracks, considering the interaction of the two rails. Each rail is represented as an infinite and uniform beam supported periodically. Additionally, identical sleepers are modeled as beams resting on a viscoelastic foundation. In the frequency domain, the track support is characterized as a spring with equivalent stiffness dependent on the mechanical properties of the beam, foundation, and rail-pad interface.

Utilizing the Floquet theorem to account for track periodicity, dynamic responses of the two rails are obtained analytically in the frequency domain using both Euler-Bernoulli and Timoshenko beam theories, with the help of Green's function. Key findings from this study include:

- In order to validate the developed work, we compare the FRFs of two rails with the existing literature where the supports are modelled as a simple mass. The similarity of the track responses are obtained, almost at the high frequency range, where the pinned-pinned frequency f_{pp}, which is the same for two models, is included. A little difference occurs at the low frequency range because of the apparition of the peaks of beam resonance (sleeper and foundation), meanwhile these values do not find in case of mass (simple support). However, the comparison allows us to validate the developed model.

- Investigation into the differences between Euler-Bernoulli and Timoshenko beam theories for the rails, revealing similar coefficients of track propagation in the low-frequency range. Discrepancies emerge around 750 Hz, nearing the pin-pin resonance of the Timoshenko beam theory, which is approximately 25 % lower than that of the Euler-Bernoulli theory. Corrections to the Euler-Bernoulli model are deemed necessary to align propagation coefficients between the two theories, particularly concerning bending wavelength, as previously noted by Nordborg.

- Comparison of forced vertical vibrations of the rails obtained from both models, indicating generally similar responses. However, at high frequencies, the Timoshenko model exhibits significant FRF attenuation along the rails, whereas the Euler-Bernoulli model shows slower decay. Additionally, the Timoshenko model predicts stronger rail vibrations, dominating other peaks on the FRFs.

These findings highlight the distinctions in FRFs of rails obtained from the two beam models. Moreover, the analytical model developed here enables rapid calculation of dynamic track responses under asymmetric load configurations, offering insights into the dynamic behaviour of railway tracks and rolling noise. Future research could explore the representation of dynamic loads to account for irregularities in wheel/rail contact, further enhancing our understanding of railway track dynamics.

Appendix A. Mathematical formulations for the beam posed on continuous foundation model

Appendix A.1. Green's function for the beam posed on a continuous foundation model

The equation of motion for the sleeper which has length $2L$ posed on a Kelvin-Voigt foundation subjected to a reaction force at position $y = y_0$ ($y_0 \in [-L, L]$) is written as:

$$B_s \frac{\partial^4 u_s}{\partial y^4} + M_s \frac{\partial^2 u_s}{\partial t^2} + k_b u_s + \zeta_b \frac{\partial u_s}{\partial t} = -R(t)\delta(y - y_0) \tag{A.1}$$

where $u_s(y, t)$ is the sleeper displacement in the time domain. The coefficients B_s, M_s are the flexural rigidity and linear mass density of sleeper, respectively. k_b and ζ_b represent the stiffness and damping coefficient of foundation, respectively. The reaction force is considered as a function in the time domain $R(t)$. By performing the Fourier's transform, the equation of motion of the sleeper is expressed in the frequency domain as follows:

$$\mathcal{L}_s\left(\hat{u}_s\right) = -\frac{\hat{R}(\omega)}{B_s}\delta(y - y_0) \tag{A.2}$$

where the mathematical operator $\mathcal{L}_s$ is defined as:

$$\mathcal{L}_s = \left[\frac{\partial^4}{\partial y^4} - \lambda_s^4\right] \tag{A.3}$$

and $\lambda_s^4 = \dfrac{M_s\omega^2 - \hat{k}_b}{B_s}$, dynamic stiffness of foundation: $\hat{k}_b = k_b + \mathrm{i}\omega\zeta_b$ and ω is the angular velocity. Eq. (A.2) describes the 4^{th} order linear differential

equation for which the analytical solution is given with the help of the Green's function $\hat{G}_s^{y_0}(y,\omega)$ as follows:

$$\hat{G}_s^{y_0}(y,\omega) = \begin{cases} M_{s_1}\cos\lambda_s y + M_{s_2}\sin\lambda_s y + M_{s_3}\cosh\lambda_s y + M_{s_4}\sinh\lambda_s y & \text{for} \quad -L \le y \le y_0 \\ N_{s_1}\cos\lambda_s y + N_{s_2}\sin\lambda_s y + N_{s_3}\cosh\lambda_s y + N_{s_4}\sinh\lambda_s y & \text{for} \quad y_0 \le y \le L \end{cases} \tag{A.4}$$

The 8 unknowns $M_{s_i}(\omega)$, $N_{s_i}(\omega)$ with $i \in [1,4]$ in Eq. (A.4) are determined to satisfy the following boundary conditions for a free-free beam subjected to a point load at position $y = y_0$:

$$\begin{cases} \dfrac{\partial^2 \hat{G}_s^{y_0}(-L,\omega)}{\partial y^2} = 0 \\ \dfrac{\partial^3 \hat{G}_s^{y_0}(-L,\omega)}{\partial y^3} = 0 \\ \dfrac{\partial^2 \hat{G}_s^{y_0}(L,\omega)}{\partial y^2} = 0 \\ \dfrac{\partial^3 \hat{G}_s^{y_0}(L,\omega)}{\partial y^3} = 0 \end{cases} \quad \text{and} \quad \begin{cases} \hat{G}_s^{y_0}(y,\omega)\Big|_{y_0^-}^{y_0^+} = 0 \\ \dfrac{\partial \hat{G}_s^{y_0}(y,\omega)}{\partial y}\Big|_{y_0^-}^{y_0^+} = 0 \\ \dfrac{\partial^2 \hat{G}_s^{y_0}(y,\omega)}{\partial y^2}\Big|_{y_0^-}^{y_0^+} = 0 \\ \dfrac{\partial^3 \hat{G}_s^{y_0}(y,\omega)}{\partial y^3}\Big|_{y_0^-}^{y_0^+} = \dfrac{1}{B_s} \end{cases} \tag{A.5}$$

The beam displacement is finally obtained in the frequency domain:

$$\hat{u}_s(y,\omega) = -\hat{R}(\omega)\hat{G}_s^{y_0}(y,\omega) \tag{A.6}$$

Appendix A.2. Mathematical transformation

Under the condition of symmetric configuration $y_{s_1} = -y_{s_2} = y_s$, the displacement of the reference sleeper ($x = 0$) at the crossing-points can be written by replacing Eq. (5) into Eq. (4):

$$\begin{cases} \hat{u}_{s_0}(y_s,\omega) = -\hat{R}_1(\omega)\hat{G}_s^{y_s}(y_s,\omega) - \hat{R}_2(\omega)\hat{G}_s^{y_s}(-y_s,\omega) \\ \hat{u}_{s_0}(-y_s,\omega) = -\hat{R}_1(\omega)\hat{G}_s^{y_s}(-y_s,\omega) - \hat{R}_2(\omega)\hat{G}_s^{y_s}(y_s,\omega) \end{cases} \tag{A.7}$$

On the other hand, the two reaction forces are also described as a function of the dynamic stiffness of the rail pad as shown in Eq. (7). So, we can deduce:

$$\begin{cases} \hat{u}_{s_0}(y_s,\omega) = \mathcal{G}_1(\omega)\hat{u}_{r_1}(0,\omega) + \mathcal{G}_2(\omega)\hat{u}_{r_2}(0,\omega) \\ \hat{u}_{s_0}(-y_s,\omega) = \mathcal{G}_2(\omega)\hat{u}_{r_1}(0,\omega) + \mathcal{G}_1(\omega)\hat{u}_{r_2}(0,\omega) \end{cases} \tag{A.8}$$

where the expressions of the two functions $\mathcal{G}_1(\omega)$ and $\mathcal{G}_2(\omega)$ are:

$$\begin{cases} \mathcal{G}_1(\omega) = \dfrac{\left[\hat{k}_{rp}\hat{G}_s^{y_s}(y_s,\omega)\left(\hat{k}_{rp}\hat{G}_s^{y_s}(-y_s,\omega)-1\right)\right] - \left[\hat{k}_{rp}\hat{G}_s^{y_s}(-y_s,\omega)\right]^2}{\left[1-\hat{k}_{rp}\hat{G}_s^{y_s}(y_s,\omega)\right]^2 - \left[\hat{k}_{rp}\hat{G}_s^{y_s}(-y_s,\omega)\right]^2} \\ \mathcal{G}_2(\omega) = \dfrac{-\hat{k}_{rp}\hat{G}_s^{y_s}(-y_s,\omega)}{\left[1-\hat{k}_{rp}\hat{G}_s^{y_s}(y_s,\omega)\right]^2 - \left[\hat{k}_{rp}\hat{G}_s^{y_s}(-y_s,\omega)\right]^2} \end{cases} \tag{A.9}$$

Appendix B. Mathematical formulations for the periodically supported beam model

Appendix B.1. Free vibration of a periodically supported Timoshenko beam

The representation of the periodically supported beam for the rail is shown in Fig. B.11. The rail is considered as an infinite beam. The dynamic load applied on the rail at position $x = x_0$. We suppose that the supports are identical and each one is modelled as an spring in the frequency domain with the dynamic stiffness $\mathcal{K}(\omega)$.

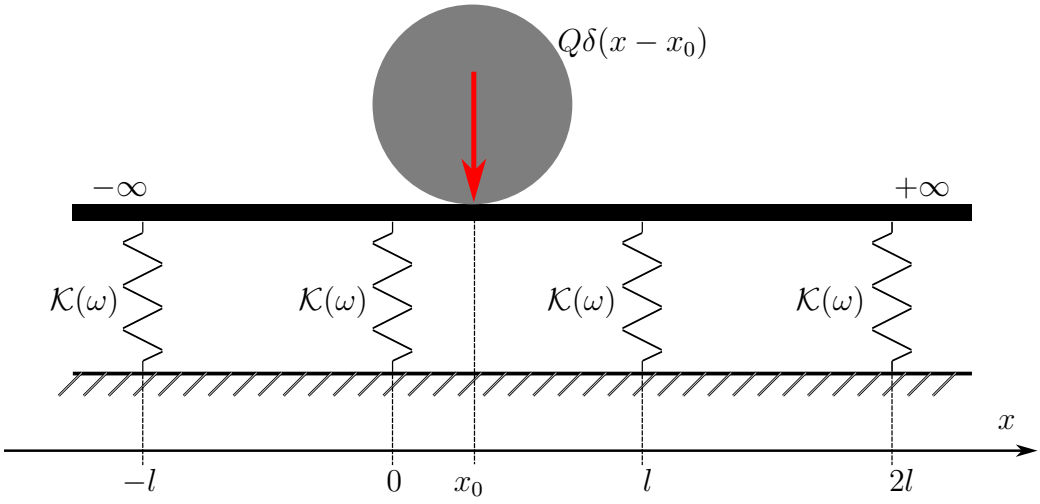

Figure B.11: Periodically supported rail model

Appendix B.1.1. Equation motion of the Timoshenko beam

The equation of motion for the rail is formulated under the influence of the external normal force $F_r(y,t)$, expressed in terms of the rail's vertical displacement $u_r(x,t)$ and rail rotation $\phi_r(x,t)$, utilizing the Timoshenko beam theory:

$$\begin{cases} M_r \dfrac{\partial^2 u_r}{\partial t^2} = K_r \left(\dfrac{\partial^2 u_r}{\partial x^2} - \dfrac{\partial \phi_r}{\partial x} \right) + F_r \\ J_r \dfrac{\partial^2 \phi_r}{\partial t^2} = B_r \dfrac{\partial^2 \phi_r}{\partial x^2} + K_r \left(\dfrac{\partial u_r}{\partial x} - \phi_r \right) \end{cases} \tag{B.1}$$

where: B_r, m_r, K_r, and J_r represent the flexural rigidity, linear mass density of the rail, shear rigidity of the rail, and rotational inertia of the rail, respectively. Upon applying Fourier's transform to Eq. (B.1), we derive the following outcomes:

$$\begin{cases} K_r \dfrac{\partial \hat{\phi}_r}{\partial x} = K_r \dfrac{\partial^2 \hat{u}_r}{\partial x^2} + M_r \omega^2 \hat{u}_r + \hat{F}_r \\ K_r \dfrac{\partial \hat{u}_r}{\partial x} = \left(K_r - J_r \omega^2 \right) \hat{\phi}_r - B_r \dfrac{\partial^2 \hat{\phi}_r}{\partial x^2} \end{cases} \tag{B.2}$$

Or we can rewrite:

$$\begin{cases} \mathcal{L}_r(\hat{u}_r) = \dfrac{1}{B_r} \left[1 - \dfrac{B_r}{K_r} \left(\dfrac{\partial^2}{\partial x^2} + \dfrac{J_r}{B_r} \omega^2 \right) \right] \hat{F}_r \\ \mathcal{L}_r(\hat{\phi}_r) = \dfrac{1}{B_r} \dfrac{\partial}{\partial x} \hat{F}_r \end{cases} \tag{B.3}$$

where the mathematical operator $\mathcal{L}_r$ is defined as:

$$\mathcal{L}_r = \left[\frac{\partial^4}{\partial x^4} + \left(\frac{J_r}{B_r} + \frac{M_r}{K_r} \right) \omega^2 \frac{\partial^2}{\partial x^2} + \frac{M_r J_r}{K_r B_r} \omega^4 - \frac{M_r}{B_r} \omega^2 \right] \tag{B.4}$$

In the context of a periodically supported rail under dynamic loads, it should be noted that the total force exerted on the beam, denoted as $F_r(x,t)$, comprises two components: the summation of reaction forces from the supports, represented as $F_s(x,t)$, and the force applied by the train, denoted as $F_t(x,t)$. Hence, the relationship is expressed as follows:

$$\begin{cases} F_r(x,t) = F_t(x,t) - F_s(x,t) & \text{in the time domain} \\ \hat{F}_r(x,\omega) = \hat{F}_t(x,\omega) - \hat{F}_s(x,\omega) & \text{in the frequency domain} \end{cases} \tag{B.5}$$

The rail/sleeper system is conceptualized as an infinite beam situated on a system of periodic supports with a spacing of l. Additionally, we make the assumption that the supports are identical, and the mechanical response of each support can be described as a linear relationship between the reaction force $\hat{R}(\omega)$ and the displacement $\hat{u}_r(x,\omega)$ through a frequency-domain stiffness $\mathcal{K}(\omega)$. In other words:

$$\hat{F}_s(x,\omega) = \sum_{n=-\infty}^{\infty} \hat{R}_n(\omega)\delta(x-nl) = \mathcal{K}(\omega)\hat{u}_r(x,\omega)\sum_{n=-\infty}^{\infty}\delta(x-nl) \quad \text{(B.6)}$$

By replacing Eq. (B.6) into Eq. (B.3), the complete problem now becomes:

$$\begin{cases} \mathcal{L}_r(\hat{u}_r) + \dfrac{\mathcal{K}}{B_r}\left[1 - \dfrac{B_r}{K_r}\left(\dfrac{\partial^2}{\partial x^2} + \dfrac{J_r}{B_r}\omega^2\right)\right]\displaystyle\sum_{n=-\infty}^{\infty}\hat{u}_r\delta(x-nl) = \frac{1}{B_r}\left[1 - \frac{B_r}{K_r}\left(\frac{\partial^2}{\partial x^2} + \frac{J_r}{B_r}\omega^2\right)\right]\hat{F}_t \\ \mathcal{L}_r(\hat{\phi}_r) + \dfrac{\mathcal{K}}{B_r}\dfrac{\partial}{\partial x}\displaystyle\sum_{n=-\infty}^{\infty}\hat{u}_r\delta(x-nl) = \frac{1}{B_r}\frac{\partial}{\partial x}\hat{F}_t \end{cases} \quad \text{(B.7)}$$

Appendix B.1.2. Free vibration of the system beam/supports

Equation (B.7) outlines a system of differential equations characterized by the periodicity of the support spacing l. Applying Floquet's theorem [54] in the absence of the train load, $\hat{F}_t(x,\omega) = 0$, the homogeneous solutions for the periodically supported Timoshenko beam are provided by:

$$\begin{cases} \hat{u}_r(x,\omega) = -\dfrac{\mathcal{K}\hat{u}_r(0,\omega)}{2B_r(\lambda_p^2+\lambda_d^2)}\left[\dfrac{C_p}{\lambda_p}\dfrac{\sin(\lambda_p(l-x)) + \mathrm{e}^{-\gamma l}\sin(\lambda_p x)}{\cos(\lambda_p l) - \cosh(\gamma l)} - \dfrac{C_d}{\lambda_d}\dfrac{\sinh(\lambda_d(l-x)) + \mathrm{e}^{-\gamma l}\sinh(\lambda_d$ \\ $\hat{\phi}_r(x,\omega) = -\dfrac{\mathcal{K}\hat{u}_r(0,\omega)}{2B_r(\lambda_p^2+\lambda_d^2)}\left[\dfrac{\cos(\lambda_p(l-x)) - \mathrm{e}^{-\gamma l}\cos(\lambda_p x)}{\cos(\lambda_p l) - \cosh(\gamma l)} - \dfrac{\cosh(\lambda_d(l-x)) - \mathrm{e}^{-\gamma l}\cosh(\lambda_d x)}{\cosh(\lambda_d l) - \cosh(\gamma l)}\right]$ \end{cases}$$

It is important to emphasize that the solution is valid solely for one period, where $x \in [0, l]$. The coefficients of Eq. (B.8) are presented in the accompanying Table B.2.

Now, assuming $x = 0$, Eq. (B.8) transforms into a 2^{nd} order equation for $\cosh\gamma$, leading to the derivation of two roots. Consequently, four propagation coefficients, $\pm\gamma_{p,d}$, are obtained, corresponding to eight homogeneous solutions: four for the displacement $\hat{u}_r(x,\omega;\pm\gamma_{p,d})$ and four for the rotational section $\hat{\phi}_r(x,\omega;\pm\gamma_{p,d})$. It is important to note that the general solution comprises a combination of these four homogeneous solutions, and $\Re(\gamma_{p,d}) \leq 0$

Coefficient	Euler-Bernoulli	Timoshenko
$\lambda_{p,d}^2$	$\sqrt{\frac{M_r\omega^2}{B_r}}$	$\sqrt{\frac{\omega^4}{4}\left(\frac{J_r}{B_r}-\frac{M_r}{K_r}\right)^2+\frac{M_r}{B_r}\omega^2}\pm\frac{\omega^2}{2}\left(\frac{J_r}{B_r}+\frac{M_r}{K_r}\right)$
$C_{p,d}$	1	$1-\frac{J_r\omega^2\mp B_r\lambda_{p,d}^2}{K_r}$

Table B.2: Coefficients for the calculation of beam responses for the two beam theories

indicates waves propagating to the right side by convention. In cases where the real part of these coefficients is zero, the wave decays, and the frequency ranges associated with this phenomenon are referred to as stop-bands.

Appendix B.2. Vertical forced vibrations of the periodically supported beam under a dynamic point-force

Appendix B.2.1. Calculation of the Green's function

By supposing that the train load $\hat{F}_t(x,\omega)$ is represented as an unit concentration force at position x_0: $\hat{F}_t(x,\omega)=\delta(x-x_0)$. The solutions of the periodically supported beam are calculated with the help of the Green's functions: the first one for the displacement $\hat{G}_{u_r}^{x_0}(x,\omega)$ and the second one for the rotational section $\hat{G}_{\phi_r}^{x_0}(x,\omega)$:

$$\begin{cases}\hat{G}_{u_r}^{x_0}(x,\omega)=\begin{cases}A_{\gamma_p}\tilde{u}_r(x,\omega;\gamma_p)+A_{\gamma_d}\tilde{u}_r(x,\omega;\gamma_d) & \text{for}\quad x\le x_0\\ A_{-\gamma_p}\tilde{u}_r(x,\omega;-\gamma_p)+A_{-\gamma_d}\tilde{u}_r(x,\omega;-\gamma_d) & \text{for}\quad x\ge x_0\end{cases}\\ \hat{G}_{\phi_r}^{x_0}(x,\omega)=\begin{cases}B_{\gamma_p}\tilde{\phi}_r(x,\omega;\gamma_p)+B_{\gamma_d}\tilde{\phi}_r(x,\omega;\gamma_d) & \text{for}\quad x\le x_0\\ B_{-\gamma_p}\tilde{\phi}_r(x,\omega;-\gamma_p)+B_{-\gamma_d}\tilde{\phi}_r(x,\omega;-\gamma_d) & \text{for}\quad x\ge x_0\end{cases}\end{cases} \tag{B.9}$$

where:

$$\begin{cases}\tilde{u}_r(x,\omega;\pm\gamma_{p,d})=\dfrac{C_p}{\lambda_p}\dfrac{\sin(\lambda_p(l-x))+\mathrm{e}^{\pm\gamma_{p,d}l}\sin(\pm\lambda_p x)}{\cos(\lambda_p l)-\cosh(\pm\gamma_{p,d}l)}-\dfrac{C_d}{\lambda_d}\dfrac{\sinh(\lambda_d(l-x))+\mathrm{e}^{\pm\gamma_{p,d}l}\sinh(\lambda_d x)}{\cosh(\lambda_d l)-\cosh(\pm\gamma_{p,d}l)}\\ \tilde{\phi}_r(x,\omega;\pm\gamma_{p,d})=\dfrac{\cos(\lambda_p(l-x))-\mathrm{e}^{\pm\gamma_{p,d}l}\cos(\lambda_p x)}{\cos(\lambda_p l)-\cosh(\pm\gamma_{p,d}l)}-\dfrac{\cosh(\lambda_d(l-x))-\mathrm{e}^{\pm\gamma_{p,d}l}\cosh(\lambda_d x)}{\cosh(\lambda_d l)-\cosh(\pm\gamma_{p,d}l)}\end{cases} \tag{B.10}$$

Here, it should be noted that Eq. (B.10) is valid only in the interval of one period of the structure, $x\in[0,l]$, as mentioned before. Out of the region,

the solutions are given as:

$$\begin{cases} \tilde{u}_r(x+nl,\omega;\pm\gamma_{p,d}) = \tilde{u}_r(x,\omega)\mathrm{e}^{\pm n\gamma_{p,d}l} & \text{for} \quad n\in\mathbb{Z} \\ \tilde{\phi}_r(x+nl,\omega;\pm\gamma_{p,d}) = \tilde{\phi}_r(x,\omega)\mathrm{e}^{\pm n\gamma_{p,d}l} & \text{for} \quad n\in\mathbb{Z} \end{cases} \tag{B.11}$$

The 8 unknowns $A_{\pm\gamma_{p,d}}(\omega)$ and $B_{\pm\gamma_{p,d}}(\omega)$ are evaluated in order to satisfy the following boundary conditions at the point-force position x_0 as follows:

$$\begin{cases} \hat{G}_{u_r}^{x_0}(x,\omega)\big|_{x_0^-}^{x_0^+} = 0 \\ \dfrac{\partial \hat{G}_{u_r}^{x_0}(x,\omega)}{\partial x}\Big|_{x_0^-}^{x_0^+} = \dfrac{-1}{K_r} \\ \dfrac{\partial^2 \hat{G}_{u_r}^{x_0}(x,\omega)}{\partial x^2}\Big|_{x_0^-}^{x_0^+} = 0 \\ \dfrac{\partial^3 \hat{G}_{u_r}^{x_0}(x,\omega)}{\partial x^3}\Big|_{x_0^-}^{x_0^+} = \dfrac{1}{B_r}\left[1+\dfrac{B_rM_r}{K_r^2}\right] \end{cases} \quad \text{and} \quad \begin{cases} \hat{G}_{\phi_r}^{x_0}(x,\omega)\big|_{x_0^-}^{x_0^+} = 0 \\ \dfrac{\partial \hat{G}_{\phi_r}^{x_0}(x,\omega)}{\partial x}\Big|_{x_0^-}^{x_0^+} = 0 \\ \dfrac{\partial^2 \hat{G}_{\phi_r}^{x_0}(x,\omega)}{\partial x^2}\Big|_{x_0^-}^{x_0^+} = \dfrac{1}{B_r} \\ \dfrac{\partial^3 \hat{G}_{\phi_r}^{x_0}(x,\omega)}{\partial x^3}\Big|_{x_0^-}^{x_0^+} = 0 \end{cases} \tag{B.12}$$

Appendix B.2.2. Solution of the complete problem

The general load is presented in complex form, consisting of two components: static and dynamic loads. The static part typically represents the mass of the train, while the dynamic part arises from track and wheel defects. In this study, the dynamic load is treated as a point force at the wheel/rail contact, formulated as follows:

$$\hat{F}_t(x,\omega) = Q\delta(x-x_0) \tag{B.13}$$

where Q is considered as a constant. Finally, the beam responses are obtained analytically in the frequency domain:

$$\begin{cases} \hat{u}_r(x,\omega) = Q\hat{G}_{u_r}^{x_0}(x,\omega) \\ \hat{\phi}_r(x,\omega) = Q\hat{G}_{\phi_r}^{x_0}(x,\omega) \\ \hat{\varepsilon}_{xx_r}(x,z_r,\omega) = -z_rQ\dfrac{\partial \hat{G}_{\phi_r}^{x_0}(x,\omega)}{\partial x} \end{cases} \tag{B.14}$$

where: $\hat{\varepsilon}_{xx_r}(x,z,\omega)$ is the beam strain in the frequency domain, z_r is the distance to the neutral axis of the beam. The first derivative of $\hat{G}_{\phi_r}^{x_0}(x,\omega)$ with regard to x is given in the following analytical form:

$$\frac{\partial \hat{G}_{\phi_r}^{x_0}(x,\omega)}{\partial x} = \begin{cases} B_{\gamma_p}\dfrac{\partial \tilde{\phi}_r(x,\omega;\gamma_p)}{\partial x} + B_{\gamma_d}\dfrac{\partial \tilde{\phi}_r(x,\omega;\gamma_d)}{\partial x} & \text{for} \quad x\le x_0 \\ B_{-\gamma_p}\dfrac{\partial \tilde{\phi}_r(x,\omega;-\gamma_p)}{\partial x} + B_{-\gamma_d}\dfrac{\tilde{\phi}_r(x,\omega;-\gamma_d)}{\partial x} & \text{for} \quad x\ge x_0 \end{cases}$$

and:

$$\frac{\partial\tilde{\phi}_r(x,\omega;\pm\gamma_{p,d})}{\partial x} = \lambda_p \frac{\sin(\lambda_p(l-x)) + \mathrm{e}^{\pm\gamma_{p,d}l}\cos(\lambda_p x)}{\cos(\lambda_p l) - \cosh(\pm\gamma_{p,d}l)} + \lambda_d \frac{\cosh(\lambda_d(l-x)) + \mathrm{e}^{\pm\gamma_{p,d}l}\cosh(\lambda_d x)}{\cosh(\lambda_d l) - \cosh(\pm\gamma_{p,d}l)}$$

Appendix C. Visualisation of the track responses

Appendix C.1. Green's functions for the railway track

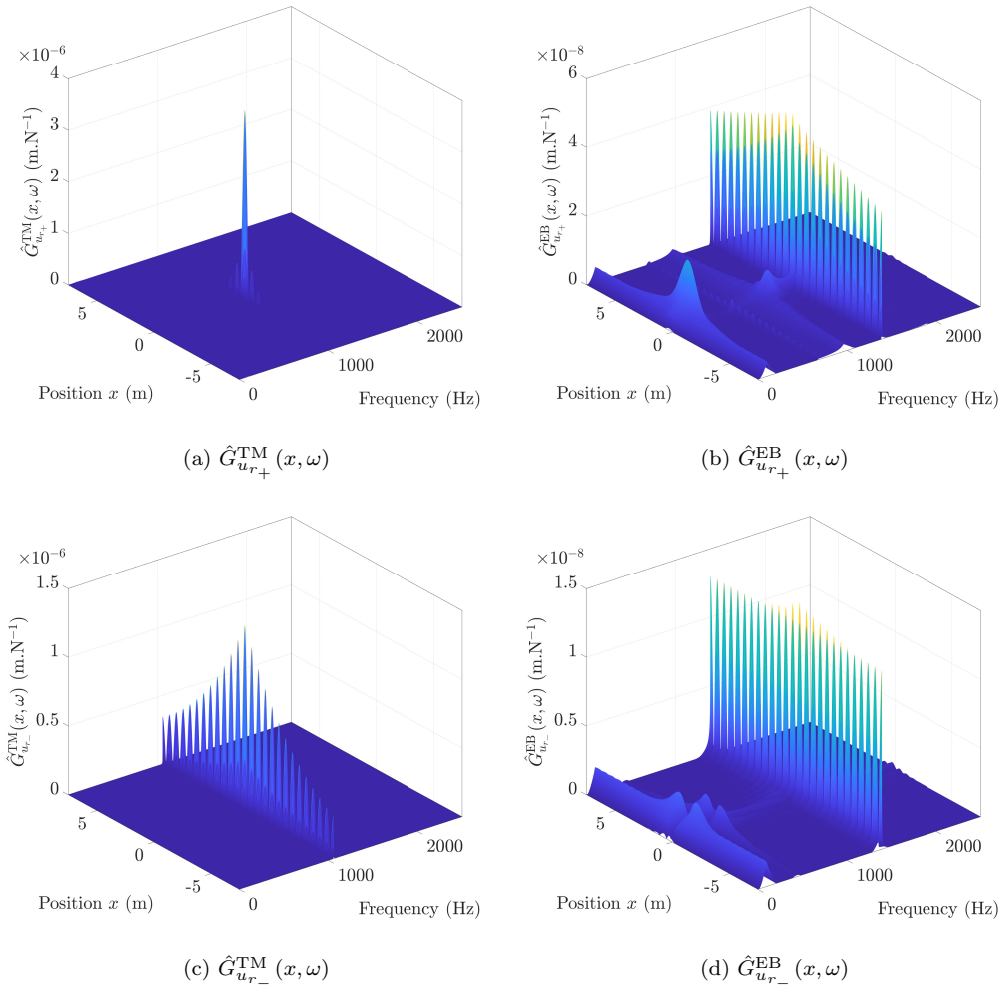

(a) $\hat{G}^{\mathrm{TM}}_{u_{r_+}}(x,\omega)$ (b) $\hat{G}^{\mathrm{EB}}_{u_{r_+}}(x,\omega)$

(c) $\hat{G}^{\mathrm{TM}}_{u_{r_-}}(x,\omega)$ (d) $\hat{G}^{\mathrm{EB}}_{u_{r_-}}(x,\omega)$

Figure C.12: Visualisation of Green's function of the railway ballasted track calculated by Eqs. (17) with two beam models: (a) $\hat{G}^{\mathrm{TM}}_{u_{r_+}}(x,\omega)$, (b) $\hat{G}^{\mathrm{EB}}_{u_{r_+}}(x,\omega)$, (c) $\hat{G}^{\mathrm{TM}}_{u_{r_-}}(x,\omega)$, and (d) $\hat{G}^{\mathrm{EB}}_{u_{r_-}}(x,\omega)$

Appendix C.2. Forced vertical vibration of rails subjected to two unit dynamic forces

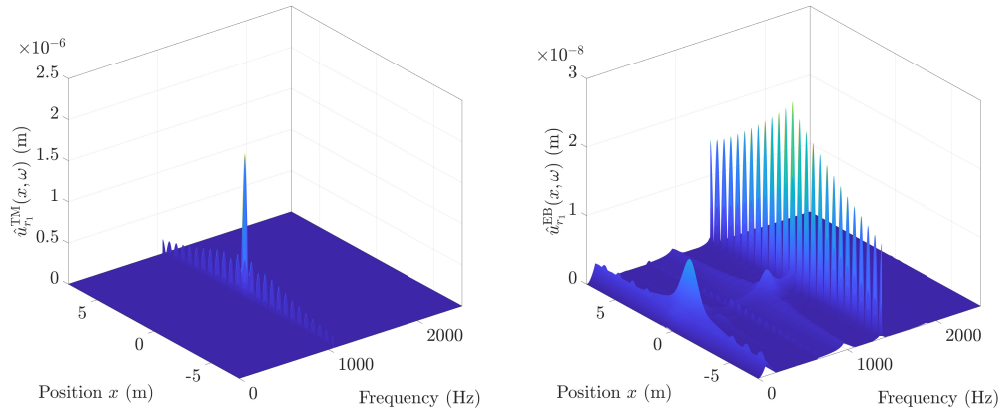

(a) $\hat{u}_{r_1}^{\mathrm{TM}}(x,\omega)$ (b) $\hat{u}_{r_1}^{\mathrm{EB}}(x,\omega)$

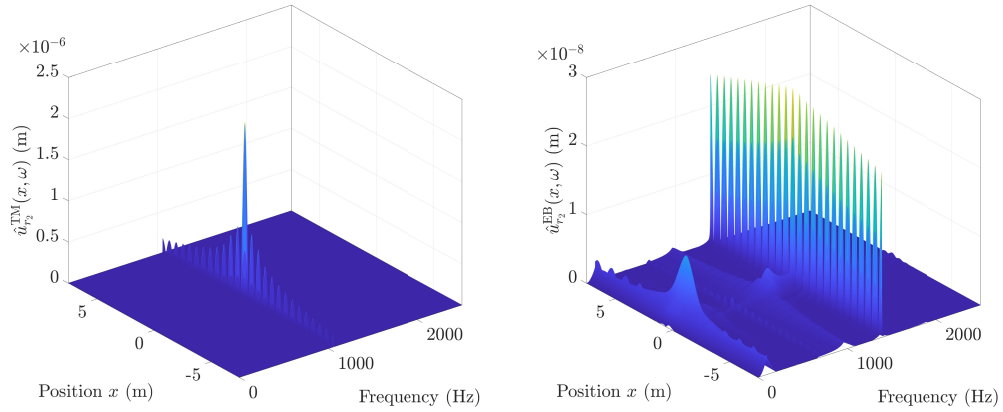

(c) $\hat{u}_{r_2}^{\mathrm{TM}}(x,\omega)$ (d) $\hat{u}_{r_2}^{\mathrm{EB}}(x,\omega)$

Figure C.13: Visualisation of forced vibration of rails under two dynamic unit forces: Q_1 at $x = 0$ and Q_2 at $x = l/2$ with two beam models: (a) $\hat{u}_{r_1}^{\mathrm{TM}}(x,\omega)$, (b) $\hat{u}_{r_1}^{\mathrm{EB}}(x,\omega)$, (c) $\hat{u}_{r_2}^{\mathrm{TM}}(x,\omega)$, and (d) $\hat{u}_{r_2}^{\mathrm{EB}}(x,\omega)$

References

[1] D. Thompson, C. Jones, A review of the modelling of wheel/rail noise generation, Journal of Sound and Vibration 231 (3) (2000) 519–536. doi:https://doi.org/10.1006/jsvi.1999.2542.

[2] L. Frýba, Vibration of solids and structures under moving loads, Springer Dordrecht, Czech, 1972.

[3] T. Hoang, D. Duhamel, G. Foret, H. Yin, P. Joyze, R. Caby, Calculation of force distribution for a periodically supported beam subjected to moving loads, Journal of Sound and Vibration 388 (2017) 327–338. doi:10.1016/j.jsv.2016.10.031.

[4] T. Hoang, D. Duhamel, G. Foret, Dynamical response of a timoshenko beams on periodical nonlinear supports subjected to moving forces, Engineering Structures 176 (2018) 673–680. doi:10.1016/j.engstruct.2018.09.028.

[5] T. Hoang, D. Duhamel, G. Foret, H.-P. Yin, G. Cumunel, Response of a periodically supported beam on a nonlinear foundation subjected to moving loads, Nonlinear Dynamics 86 (2) (2016) 953–961. doi:10.1007/s11071-016-2936-5.

[6] L.-H. Tran, T. Hoang, D. Duhamel, G. Foret, S. Messad, A. Loaec, A Fast Analytic Method to Calculate the Dynamic Response of Railways Sleepers, Journal of Vibration and Acoustics 141 (1), 011005 (08 2018). doi:10.1115/1.4040392.

[7] L.-H. Tran, K. Le-Nguyen, T. Hoang, A comparison of beam models for the dynamics of railway sleepers, International Journal of Rail Transportation 11 (1) (2023) 92–110. doi:10.1080/23248378.2022.2034062.

[8] L.-H. Tran, T.-T.-. Do, K. Le-Nguyen, Influence of beam models on dynamic responses of ballasted railway track subjected to moving loads, Archive of Applied Mechanics 93 (2023) 3665–3682. doi:10.1007/s00419-023-02459-4.

[9] L.-H. Tran, K. Le-Nguyen, Calculation of dynamic responses of a cracked beam on visco-elastic foundation subjected to moving loads, and its application to a railway track model, International Journal of Applied Mechanics 15 (03) (2023) 2350026. doi:10.1142/S1758825123500266.

[10] S. Kaewunruen, A. M. Remennikov, Dynamic flexural influence on a railway concrete sleeper in track system due to a single wheel impact,

Engineering Failure Analysis 16 (3) (2009) 705–712. doi:10.1016/j.engfailanal.2008.06.002.

[11] S. Kaewunruen, C. Ngamkhanong, C. H. Lim, Damage and failure modes of railway prestressed concrete sleepers with holes/web openings subject to impact loading conditions, Engineering Structures 176 (2018) 840–848. doi:10.1016/j.engstruct.2018.09.057.

[12] S. Grassie, Dynamic modelling of concrete railway sleepers, Journal of Sound and Vibration 187 (5) (1995) 799–813. doi:10.1006/jsvi.1995.0564.

[13] J. Park, S. Ahn, J. Kim, H.-I. Koh, J. Park, Direct determination of dynamic properties of railway tracks for flexural vibrations, European Journal of Mechanics - A/Solids 61 (2017) 14–21. doi:10.1016/j.euromechsol.2016.08.010.

[14] R. Janeliukstis, S. Ručevskis, S. Kaewunruen, Mode shape curvature squares method for crack detection in railway prestressed concrete sleepers, Engineering Failure Analysis 105 (2019) 386–401. doi:10.1016/j.engfailanal.2019.07.020.

[15] A. Nordborg, Vertical rail vibrations: Pointforce excitation, Acta Acustica 84 (1998) 280–288.

[16] A. Nordborg, Vertical rail vibrations: Parametric excitation, Acta Acustica 84 (1998) 289–300.

[17] A. Nordborg, Wheel/rail noise generation due to nonlinear effects and parametric excitation, The Journal of the Acoustical Society of America 111 (4) (2002) 1772–1781. doi:10.1121/1.1459463.

[18] A. Nordborg, H.-I. Koh, Comparison of two different models describing railway noise generation and radiation, 2017, pp. 7527–7536, interNoise16.

[19] A. Nordborg, Rail/wheel rolling noise generation due to parametric excitation, Journal of Vibration and Control 27 (23-24) (2021) 2862–2869. doi:10.1177/1077546320968650.

[20] J.-F. Hamet, Railway noise: Use of the timoshenko model in rail vibration studies, Acta Acustica 85 (1999) 54–62.

[21] M. A. Heckl, Railway noise - can random sleeper spacings helps ?, Acustica 81 (1995) 559–564.

[22] S. L. Grassie, R. W. Gregory, D. Harrison, K. L. Johnson, The dynamic response of railway track to high frequency vertical excitation, Journal of Mechanical Engineering Science 24 (2) (1982) 77–90. doi:10.1243/JMES_JOUR_1982_024_016_02.

[23] S. L. Grassie, R. W. Gregory, K. L. Johnson, The dynamic response of railway track to high frequency lateral excitation, Journal of Mechanical Engineering Science 24 (2) (1982) 91–95. doi:10.1243/JMES_JOUR_1982_024_017_02.

[24] K. L. Knothe, S. Grassie, Modelling of railway track and vehicle/track interaction at high frequencies, Vehicle System Dynamics 22 (3-4) (1993) 209–262. doi:10.1080/00423119308969027.

[25] D. Mead, Free wave propagation in periodically supported, infinite beams, Journal of Sound and Vibration 11 (2) (1970) 181–197. doi:10.1016/S0022-460X(70)80062-1.

[26] D. Mead, A new method of analyzing wave propagation in periodic structures; applications to periodic timoshenko beams and stiffened plates, Journal of Sound and Vibration 104 (1) (1986) 9–27. doi:10.1016/S0022-460X(86)80128-6.

[27] D. Mead, The response of infinite periodic beams to point harmonic forces: A flexural wave analysis, Journal of Sound and Vibration 144 (3) (1991) 507–529. doi:10.1016/0022-460X(91)90565-2.

[28] D. Mead, Wave propagation in continuous periodic structures : Research contributions from southampton, 1964-1995, Journal of Sound and Vibration 190 (3) (1996) 495–524. doi:10.1006/jsvi.1996.0076.

[29] Y. Zhang, X. Liu, Y. Wei, Response of an infinite beam on a bilinear elastic foundation: Bridging the gap between the winkler and tensionless foundation models, European Journal of Mechanics - A/Solids 71 (2018) 394–403. doi:10.1016/j.euromechsol.2018.06.006.

[30] A. Kumawat, P. Raychowdhury, S. Chandra, A wave number based approach for the evaluation of the green's function of a one-dimensional railway track model, European Journal of Mechanics - A/Solids 78 (2019) 103854. doi:https://doi.org/10.1016/j.euromechsol.2019.103854.

[31] L.-H. Tran, T.-M. Duong, T. Hoang, G. Foret, D. Duhamel, An analytical model to calculate the forced vertical vibrations of two rails subjected to the dynamic loads of ballasted railway track, Structures 68 (2024) 107203. doi:10.1016/j.istruc.2024.107203.

[32] K. Knothe, Z. Strzyzakowski, K. Willner, Rail vibrations in the high frequency range, Journal of Sound and Vibration 169 (1) (1994) 111–123. doi:https://doi.org/10.1006/jsvi.1994.1009.

[33] L. Gavrić, Computation of propagative waves in free rail using a finite element technique, Journal of Sound and Vibration 185 (3) (1995) 531–543. doi:https://doi.org/10.1006/jsvi.1995.0398.

[34] L. Gry, Dynamic modelling of railway track based on wave propagation, Journal of Sound and Vibration 195 (3) (1996) 477–505. doi:https://doi.org/10.1006/jsvi.1996.0438.

[35] L. Gry, C. Gontier, Dynamic modelling of railway track: A periodic model based on a generalized beam formulation, Journal of Sound and Vibration 199 (4) (1997) 531–558. doi:https://doi.org/10.1006/jsvi.1995.0671.

[36] G. Guo, C. Hao, B. Du, Static and dynamic response characteristics of a ballastless track structure of a high-speed railway bridge with interlayer debonding under temperature loads, Engineering Failure Analysis 151 (2023) 107377. doi:10.1016/j.engfailanal.2023.107377.

[37] J. Luo, S. Zhu, Z. Zeng, W. Zhai, Semi-analytical solution for interfacial debonding of high-speed railway ballastless track under thermal loading using a quasi-dynamic method, Applied Mathematical Modelling 121 (2023) 339–363. doi:10.1016/j.apm.2023.05.006.

[38] J. Sadeghi, M. Fesharakif, Importance of nonlinearity of track support system in modeling of railway track dynamics, International Journal

of Structural Stability and Dynamics 13 (01) (2013) 1350008. doi:10.1142/S0219455413500089.

[39] J. Ruiz, P. Alves Costa, R. Calçada, L. Rodríguez, A. Colaço, Study of ground vibrations induced by railway traffic in a 3d fem model formulated in the time domain: experimental validation, Structure and Infrastructure Engineering (2016) 1–13doi:10.1080/15732479.2016.1172649.

[40] Q. Jin, D. J. Thompson, D. E. Lurcock, M. G. Toward, E. Ntotsios, A 2.5d finite element and boundary element model for the ground vibration from trains in tunnels and validation using measurement data, Journal of Sound and Vibration 422 (2018) 373–389. doi:10.1016/j.jsv.2018.02.019.

[41] M. Hussein, S. François, M. Schevenels, H. Hunt, J. Talbot, G. Degrande, The fictitious force method for efficient calculation of vibration from a tunnel embedded in a multi-layered half-space, Journal of Sound and Vibration 333 (25) (2014) 6996–7018. doi:10.1016/j.jsv.2014.07.020.

[42] E. Ntotsios, D. Thompson, M. Hussein, The effect of track load correlation on ground-borne vibration from railways, Journal of Sound and Vibration 402 (2017) 142–163. doi:10.1016/j.jsv.2017.05.006.

[43] S. Koroma, D. Thompson, M. Hussein, E. Ntotsios, A mixed space-time and wavenumber-frequency domain procedure for modelling ground vibration from surface railway tracks, Journal of Sound and Vibration 400 (2017) 508–532. doi:10.1016/j.jsv.2017.04.015.

[44] E. Ntotsios, D. J. Thompson, M. F. Hussein, A comparison of ground vibration due to ballasted and slab tracks, Transportation Geotechnics 21 (2019) 100256. doi:10.1016/j.trgeo.2019.100256.

[45] G. K. David J. Thompson, E. Ntotsios, Modelling, simulation and evaluation of ground vibration caused by rail vehicles*, Vehicle System Dynamics 57 (7) (2019) 936–983. doi:10.1080/00423114.2019.1602274.

[46] M. Germonpré, G. Degrande, G. Lombaert, A study of modelling simplifications in ground vibration predictions for railway traffic at grade,

Journal of Sound and Vibration 406 (2017) 208–223. doi:10.1016/j.jsv.2017.06.022.

[47] L.-H. Tran, T. Hoang, D. Duhamel, G. Foret, S. Messad, A. Loaec, Influence of non-homogeneous foundations on the dynamic responses of railway sleepers, International Journal of Structural Stability and Dynamics 21 (01) (2021) 2150002. doi:10.1142/S0219455421500024.

[48] L.-H. Tran, T. Hoang, G. Foret, D. Duhamel, Calculation of the dynamic responses of a railway track on a non-uniform foundation, Journal of Vibration and Control 29 (15-16) (2023) 3544–3553. doi:10.1177/10775463221099353.

[49] L.-H. Tran, T. Hoang, G. Foret, D. Duhamel, D.-D. Nguyen, Calculation of dynamic responses of railway sleepers on a nonlinear foundationhod, Nonlinear Dynamics 112 (1) (2024) 443–458. doi:10.1007/s11071-023-09070-w.

[50] B. Claudet, T. Hoang, D. Duhamel, G. Foret, J.-L. Pochet, F. Sabatier, Wave finite element method for computing the dynamic reponses of railway transition zones subjected to moving loads, 2019, pp. 4538–4547. doi:10.7712/120119.7247.18688.

[51] Y. Chi, K. Korkut, S. Salvatore, Investigation of wave propagation and attenuation in periodic supported rails using wave finite element method, Acta Mechanica 235 (3) (2024) 1453–1469. doi:10.1007/s00707-023-03484-8.

[52] U. J. Kurze, Refined calculations or improved understanding of rail vibrations citation ?, Acta Acustica 83 (1997) 506–515.

[53] D. Thompson, Railway Noise and Vibration, 1st Edition, Elsevier, 2008.

[54] P. A. Kunchment, Floquet theory for partial differential equations, in: Operator Theory: Advances and Applications, 1st Edition, Vol. 60, Birchauser, Basel, 1993.